

FORSCHUNGSZENTRUM KARLSRUHE

Technik und Umwelt

Wissenschaftliche Berichte

FZKA 6057

A compendium of T-stress solutions

T. Fett

Institut für Materialforschung

Forschungszentrum Karlsruhe GmbH, Karlsruhe

1998

A compendium of T-stress solutions

Abstract:

The failure of cracked components is governed by the stresses in the vicinity of the crack tip. The singular stress contribution is characterised by the stress intensity factor K , the first regular stress term is represented by the so-called T-stress.

T-stress solutions for components containing two-dimensional internal cracks and edge cracks were computed by application of the Boundary Collocation Method (BCM). The results are compiled in form of tables, diagrams or approximative relations.

In addition a Green's function for T-stresses is proposed for internal and external cracks which enables to compute T-stress terms for any given stress distribution in the uncracked body.

Eine Sammlung von T-Spannungs-Lösungen

Kurzfassung:

Das Versagen von Bauteilen mit Rissen wird durch die unmittelbar an der Rispitze auftretenden Spannungen verursacht. Der singuläre Anteil diese Spannungen wird durch den Spannungsintensitätsfaktor K charakterisiert. Der erste reguläre Term wird durch die sogenannte T-Spannung beschrieben.

Im vorliegenden Bericht werden Ergebnisse für Bauteile mit zweidimensionalen Innenrissen sowie Außenrissen mitgeteilt, die mit der "Boundary Collocation Methode" (BCM) bestimmt wurden. Die Resultate werden in Form von Tabellen, Diagrammen und Näherungsformeln wiedergegeben.

Zusätzlich wurden Greensfunktionen für Innen- und Außenrisse angegeben. Diese erlauben die Berechnung des T-Spannungsterms für beliebige Spannungsverteilungen in der ungerissenen Struktur.

Contents

1	Introduction	1
2	T-stress term	2
I METHODS		
3	Green's function for T-stress	6
3.1	Representation of T-stresses by a Green's function	6
3.2	Set-up for the Green's function	7
3.2.1	Asymptotic term	7
3.2.2	Correction terms for the Green's function	9
3.2.2.1	Edge cracks	9
3.2.2.2	Internal cracks	10
4	Boundary Collocation Procedure	11
4.1	Boundary conditions	11
4.2	Stress function for point forces	14
5	Principle of superposition	17
II RESULTS		
6	Crack in an infinite body	20
6.1	Couples of forces	20
6.2	Constant crack face loading	21
7	Circular disk with internal crack	22
7.1	Constant internal pressure	22
7.2	Disk partially loaded by normal tractions	24
7.3	Central point force on the crack face	26

8 Estimation of T-terms with a Green's function	28
8.1 Green's function with one regular term	28
8.2 Green's function with two regular terms	30
9 Rectangular plate with internal crack	32
9.1 T-stress for pure tensile load	32
10 Edge-cracked rectangular plate	34
10.1 Rectangular plate under tension	34
10.2 Rectangular plate under bending load	35
10.3 Edge-cracked bar in 3-point bending	39
10.4 The Double Cantilever Beam (DCB) specimen	41
10.5 Couple of opposite point forces	42
10.6 Rectangular plate with thermal stresses	44
10.7 Partially loaded edge-cracked rectangular plate	46
11 Edge-cracked circular disk	51
11.1 Circumferentially loaded disk	51
11.2 Diametrically loaded disk	51
11.2.1 Load perpendicular to the crack	52
11.2.2 Brazilian disk (edge-cracked)	55
11.2.3 Disk with thermal stresses	57
12 Cracks ahead of notches	60
13 Array of deep edge cracks	64
14 Double-edge-cracked plate	66
15 Double-edge-cracked circular disk	68
16 References	71

1 Introduction

The fracture behaviour of cracked structures is dominated by the near-tip stress field. In fracture mechanics, interest focusses on stress intensity factors, which describe the singular stress field ahead of a crack tip and govern fracture of a specimen when a critical stress intensity factor is reached. Nevertheless, there is experimental evidence (e.g. [1-3]) that also the constant stress contributions acting over a longer distance from the crack tip may affect fracture mechanics properties. Sufficient information about the stress state is available, if the stress intensity factor and the constant stress term, the T-stress, are known.

While stress intensity factor solutions are reported in handbooks for many crack geometries and loading cases, T-stress solutions are available only for a small number of test specimens and simple loading cases as for instance pure tension and bending.

Different methods were applied in the past to compute the T-stress term for fracture mechanics standard test specimens. Regarding one-dimensional cracks, Leever and Radon [4] made a numerical analysis based on a variational method. Kfoury [5] applied the Eshelby technique. Sham [6,7] developed a second-order weight function based on a work-conjugate integral and evaluated it for the SEN specimen using the FE method. In [8,9] a Green's function for T-stresses was determined on the basis of Boundary Collocation results. Wang and Parks [10] extended the T-stress evaluation to two-dimensional surface cracks using the line-spring method.

In earlier reports the T-stress term for single edge-cracked structures [11] and for double-edge cracked plates [12] were communicated. In [13] the computations were extended to internal one-dimensional cracks.

In the present report all the T-stress solutions are compiled. Most of the results were obtained with the Boundary Collocation Procedure and with the Green's function technique. Therefore, these methods are described in detail in Sections 2-4. Section 5 contains solutions for internal cracks and Section 6 represents results for edge cracks.

2 T-stress term

The complete stress state in a cracked body is known if a related stress function is known. In most cases, the Airy stress function Φ is an appropriate tool which results as the solution of

$$\Delta\Delta\Phi = 0 \quad (2.1)$$

For a cracked body a series representation for Φ was given by Williams [14]. Its symmetric part can be written in polar coordinates with the crack tip as the origin

$$\begin{aligned} \Phi = \sigma^* W^2 \sum_{n=0}^{\infty} (r/W)^{n+3/2} A_n \left[\cos(n + \frac{3}{2})\varphi - \frac{n + \frac{3}{2}}{n - \frac{1}{2}} \cos(n - \frac{1}{2})\varphi \right] \\ + \sigma^* W^2 \sum_{n=0}^{\infty} (r/W)^{n+2} A_n^* [\cos(n+2)\varphi - \cos n\varphi] \end{aligned} \quad (2.2)$$

where σ^* is a characteristic stress and W is a characteristic dimension. The geometric data are explained by Fig. 2.1.

From this stress function the x-component of the stresses results at $\varphi=0$

$$\sigma_x / \sigma^* = - \sum_{n=0}^{\infty} A_n \left(\frac{a-x}{W} \right)^{n-1/2} \frac{(2n+3)(2n+1)}{2n-1} - \sum_{n=0}^{\infty} 4A_n^* \left(\frac{a-x}{W} \right)^n (n+1) \quad (2.3)$$

The term with coefficient A_0 is related to the stress intensity factor K_I by

$$K_I = \sigma^* F \sqrt{\pi a} \quad (2.4)$$

with the geometric function F

$$F = A_0 \sqrt{18/\alpha} \quad , \quad \alpha = a/W \quad (2.5)$$

The term with coefficient A_0^* represents the total constant σ_x -stress contribution appearing at the crack tip ($x=a$) of a cracked structure

$$\sigma_x|_{x=a} = -4\sigma^* A_0^* \quad (2.6)$$

This total x-stress includes stress contributions which are already present at the location $x=a$ in the uncracked body, $\sigma_{x,a}^{(0)}$, and an additional stress term which is generated by the crack exclusively. This contribution of the crack is called the T-stress and given by

$$T = -4\sigma^* A^*_0 - \sigma^{(0)}_{x,a} \quad (2.7)$$

The total x-stress component is also of interest for fracture mechanics considerations. This may give rise to defining an additional T-term, T' , by

$$T' = T + \sigma^{(0)}_{x,a} = -4\sigma^* A^*_0 \quad (2.8)$$

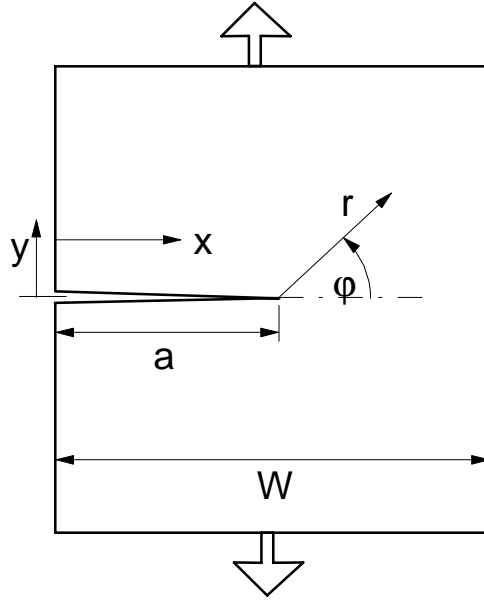


Fig. 2.1 Geometrical data of a crack in a component.

Leevers and Radon [4] proposed a dimensionless representation by the stress biaxiality ratio β

$$\beta = \frac{T\sqrt{\pi a}}{K_I} = \frac{T}{\sigma^* F} \quad (2.9)$$

Taking into consideration the singular stress term and the first regular term, the near-tip stress field can be described by

$$\sigma_{ij} = \frac{K_I}{\sqrt{2\pi a}} f_{ij}(\varphi) + \sigma_{ij,0} \quad (2.10)$$

$$\sigma_{ij,0} = \begin{pmatrix} \sigma_{xx,0} & \sigma_{xy,0} \\ \sigma_{yx,0} & \sigma_{yy,0} \end{pmatrix} = \begin{pmatrix} T & 0 \\ 0 & 0 \end{pmatrix} \quad (2.11)$$

where f_{ij} are the well-known angular functions for the singular stress contribution.

I METHODS

For the determination of T-stress solutions the following methods were applied:

- Westergaard stress function
- Williams (Airy) stress function
- Boundary Collocation method
- Green's function method
- Principle of superposition.

The methods are outlined in Sections 3 and 4.

3 Green's function for T-stress

3.1 Representation of T-stresses by a Green's function

As a consequence of the principle of superposition, stress fields for different loadings can be added in the case of single loadings acting simultaneously. This leads to an integration representation of the loading parameters and was applied very early to the singular stress field and the computation of the related stress intensity factor by Bückner [15]. Similarly, the T-stress term can be expressed by an integral [6-9]. The integral representations read

$$K_I = \int_0^a h(x, a) \sigma_y(x) dx \quad , \quad T = \int_0^a t(x, a) \sigma_y(x) dx \quad (3.1)$$

where the integration has to be performed with the stress field σ_y in the uncracked body (Fig.3.1). The stress contributions are weighted by a weight function (h, t) dependent on the location x where the stress σ_y acts.

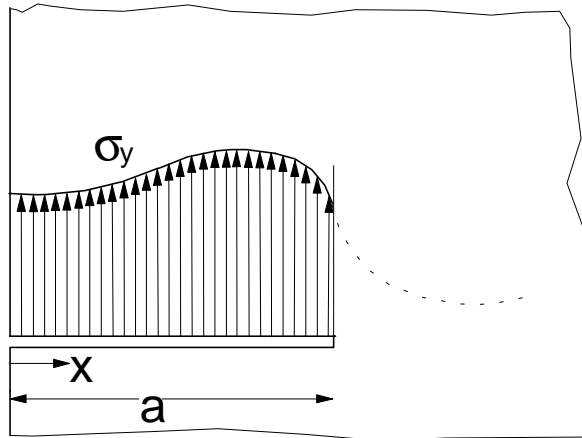


Fig. 3.1 Crack loaded by continuously distributed normal tractions (present in the uncracked body).

The weight functions h and t can be interpreted as the stress intensity factor and as the T-term for a pair of single forces P acting at the crack face at the location x_0 (Fig.3.2), i.e. the weight functions (h, t) are Green's functions for K_I and T . This can be shown easily. The single forces are represented by a stress distribution

$$\sigma(x) = \frac{P}{B} \delta(x - x_0) \quad (3.2)$$

where δ is the Dirac Delta-function and B is the thickness of the plate (often chosen to be $B=1$). By introducing these stress distribution into (3.2) we obtain

$$K_p = \frac{P}{B} \int_0^a \delta(x - x_0) h(x, a) dx = \frac{P}{B} h(x_0, a) \quad (3.3a)$$

$$T_p = \frac{P}{B} \int_0^a \delta(x - x_0) t(x, a) dx = \frac{P}{B} t(x_0, a) \quad (3.3b)$$

i.e. the weight function terms $h(x_0, a)$ and $t(x_0, a)$ are the Green's functions for the stress intensity factor and T-stress term.

3.2 Set-up of the Green's function

3.2.1 Asymptotic term

In order to describe the Green's function, a separation is made consisting of a term t_0 representing the asymptotic limit case of near-tip behaviour and a correction term t_{corr} which includes information about the special shape of the component and the finite dimensions,

$$t = t_0 + t_{corr} \quad (3.4)$$

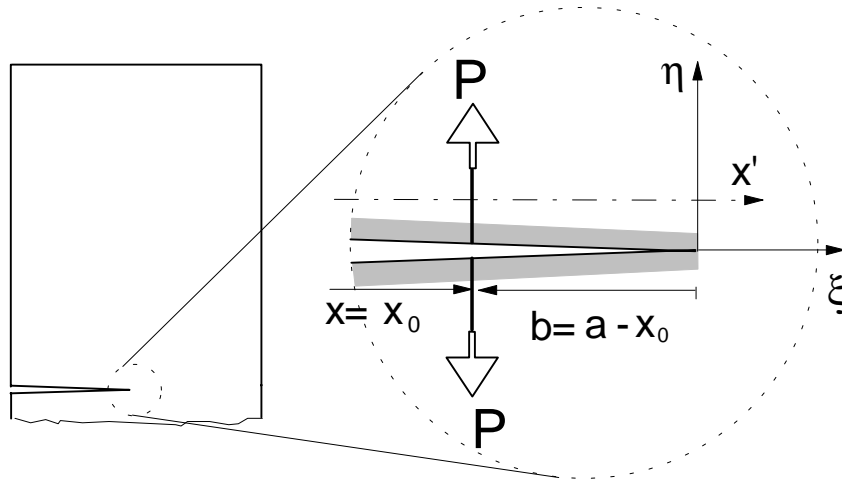


Fig. 3.2 Situation at the crack tip for asymptotic stress consideration.

In order to obtain information on the asymptotic behaviour of the weight or Green's function, we consider exclusively the near-tip behaviour. Therefore, we take into consideration a small section of the body (dashed circle) very close to the crack tip (Fig.3.2). The near-tip zone is zoomed very strongly. Consequently, the outer borders of the component move to infinity.

Now, we have the case of a semi-infinite crack in an infinite body. If we load the crack faces by a couple of forces P at location $x=x_0 \ll a$, the stress state can be described in terms of the Westergaard stress function [16]:

$$Z = \frac{P}{\pi} \frac{1}{z+b} \sqrt{\frac{b}{z}} \quad , \quad z = \xi + i\eta \quad (3.5)$$

The regular contribution to the stress function is ($z, b \neq 0$)

$$Z_{reg} = -\frac{P}{\pi} \frac{1}{z+b} \sqrt{\frac{z}{b}} \quad (3.6)$$

from which the regular part of the x-stress component results as

$$\sigma_x = \operatorname{Re} Z - y \operatorname{Im}(dZ/dz) \Rightarrow \sigma_x|_{y=0} = \operatorname{Re}\{Z\}|_{y=0} \quad (3.7)$$

$$\sigma_{x,reg}|_{y=0} = \operatorname{Re}\{Z_{reg}\}|_{y=0} = -\frac{P}{\pi} \frac{\sqrt{x'-a}}{(x'-x)\sqrt{a-x}} \quad , \quad x' > a \quad (3.8)$$

The constant x-stress term, i.e. the regular x-stress at $x'=0$ is then given by

$$\sigma_{x,reg}|_{x \rightarrow 0} = -\frac{P}{\pi} \lim_{x' \rightarrow a} \frac{\sqrt{x'-a}}{(x'-x)\sqrt{a-x}} \quad (3.9)$$

and the Green's function reads

$$\Rightarrow t_0 = -\frac{1}{\pi} \lim_{x' \rightarrow a} \frac{\sqrt{x'-a}}{(x'-x)\sqrt{a-x}} \quad (3.10)$$

From (3.9), the T-stress can be derived for a couple of forces for a semi-infinite crack in an infinite body, namely

$$T = \begin{cases} 0 & \text{for } x < a \\ \infty & \text{for } x = a \end{cases} \quad (3.11)$$

Let us consider the crack loading p to be represented by a Taylor series with respect to the crack tip as

$$p(x) = p|_{x=a} - \frac{dp}{dx}|_{x=a} (a-x) + \frac{1}{2} \frac{d^2p}{dx^2}|_{x=a} (a-x)^2 + \dots \quad (3.12)$$

The corresponding T-stress contribution, resulting from the asymptotic part of the Green's function, is given by

$$T_0 = \int_0^a t_0(x', a, x) \sigma(x) dx = -\frac{1}{\pi} \sigma_y \Big|_{x=a} \lim_{x' \rightarrow a} \sqrt{x'-a} \int_0^a \frac{dx}{(x'-x)\sqrt{a-x}} + R \quad (3.13)$$

with the remainder R containing integrals of the type

$$I_n = \int_0^a \frac{(a-x)^{n-1/2}}{x'-x} dx, \quad n \geq 1 \quad (3.14)$$

which yield (see e.g. integral 212.14a in [17])

$$I_n = 2 \sum_{v=0}^{n-1} \frac{(a-x')^v}{2n-1-2v} a^{n-v-1/2} + a^{n-1/2} \ln \frac{\sqrt{a}-\sqrt{x'-a}}{\sqrt{a}+\sqrt{x'-a}} \quad (3.15)$$

Consequently, the limit value is

$$\lim_{x' \rightarrow a} \sqrt{x'-a} I_n = 0 \Rightarrow R = 0 \quad (3.16)$$

and the term T_0 is exclusively represented by the first integral term in (3.13). Integration of this term results in

$$\begin{aligned} -\frac{1}{\pi} p \Big|_{x=a} \lim_{x' \rightarrow a} \sqrt{x'-a} \int_0^a \frac{dx}{(x'-x)\sqrt{a-x}} &= -\frac{1}{\pi} p \Big|_{x=a} \lim_{x' \rightarrow a} \sqrt{x'-a} \left[\frac{2}{\sqrt{x'-a}} \arctan \sqrt{\frac{x'-a}{a-x}} \right]_0^a = \\ &= -\frac{1}{\pi} p \Big|_{x=a} \lim_{x' \rightarrow a} \left[\pi - \arctan \sqrt{\frac{x'-a}{a}} \right] = -p \Big|_{x=a} \end{aligned} \quad (3.17)$$

$$\Rightarrow T_0 = -p \Big|_{x=a} = -\sigma_y \Big|_{x=a} \quad (3.18)$$

3.2.2 Correction terms for the Green's function

3.2.2.1 Edge cracks

By the considerations made before, only the asymptotic part of the x-stress is derived. Since a small region around the crack tip was chosen, the component boundaries were shifted to infinity. Now, a set-up has to be chosen for the weight function contribution t_{corr} which includes the finite size of the component.

Let us assume the difference between the complete Green's function $t(b)$ and its asymptotic part $t_0(b)$ to be expressible in a Taylor series for $b=a-x \rightarrow 0$

$$t_{\text{corr}}(b) = t(b) - t_0(b) = f(b) = 0 + \frac{\partial t}{\partial b} \Big|_{b=0} b + \frac{1}{2} \frac{\partial^2 t}{\partial b^2} \Big|_{b=0} b^2 + \dots \quad (3.19)$$

Then the complete Green's function can be written as

$$t = t_0 + \sum_{v=1}^{\infty} C_v (1 - x/a)^v \quad (3.20)$$

If we restrict the expansion to the leading term, we obtain as an approximation

$$t \cong t_0 + C \left(1 - \frac{x}{a}\right) \quad (3.21)$$

A simple procedure to determine approximative Green's functions is possible by determination of the unknown coefficients in the series representation (3.20) to known T-solutions for reference loading cases [9]. The general treatment may be shown for the determination of the coefficient C for an approximative weight function representation according to (3.21).

Let us assume the T-term T_t of a centrally cracked plate under pure tension σ_0 to be known. Introducing (3.21) into (3.1) yields

$$T = \sigma_0 \int_0^a t(x, a) dx = \sigma_0 \int_0^a t_0 dx + \sigma_0 C \int_0^a (1 - x/a) dx = \sigma_0 \left(-1 + C \frac{a}{2}\right) \quad (3.22)$$

and the coefficient C results as

$$C = \frac{2}{a} \left(1 + \frac{T_t}{\sigma_0}\right) \quad (3.23)$$

Knowledge of additional reference solutions for T allows to determine further coefficients.

3.2.2.2 Internal crack

The derivation of an approximate Green's function for internal cracks is similar to those of edge cracks. Due to the symmetry at $x=0$, the general set-up must be modified. An improved description that fulfills eq.(3.19) and is symmetric with respect to $x=0$ is

$$t = t_0 + \sum_{v=1}^{\infty} C_v (1 - x^2/a^2)^v \quad (3.24)$$

with the first approximation

$$t \cong t_0 + C(1 - x^2/a^2) \quad (3.25)$$

In this case, the coefficient C results from the pure tension case as

$$C = \frac{3}{2a} \left(1 + \frac{T_t}{\sigma_0}\right) \quad (3.26)$$

4 Boundary Collocation Procedure

4.1 Boundary conditions

A simple possibility to determine the coefficients A_0 and A^*_0 is the application of the Boundary Collocation Method (BCM) [18-20]. For practical application of eq.(2), which is used to determine A_0 and A^*_0 , the infinite series for the Airy stress function must be truncated after the N th term for which an adequate value must be chosen. The still unknown coefficients are determined by fitting the stresses and displacements to the specified boundary conditions. The stresses result from the relations

$$\sigma_r = \frac{1}{r} \frac{\partial \Phi}{\partial r} + \frac{1}{r^2} \frac{\partial^2 \Phi}{\partial \varphi^2} \quad (4.1)$$

$$\sigma_\varphi = \frac{\partial^2 \Phi}{\partial r^2} \quad (4.2)$$

$$\tau_{r\varphi} = \frac{1}{r^2} \frac{\partial \Phi}{\partial \varphi} - \frac{1}{r} \frac{\partial^2 \Phi}{\partial r \partial \varphi} \quad (4.3)$$

The displacements read in terms of the Williams stress function

$$\begin{aligned} \frac{u_x}{\sigma^* W} &= \frac{1+\nu}{E} \sum_{n=0}^{\infty} A_n \left(\frac{r}{W} \right)^{n+1/2} \frac{2n+3}{2n-1} [(n+4\nu-\frac{5}{2}) \cos(n-\frac{1}{2})\varphi - (n-\frac{1}{2}) \cos(n+\frac{3}{2})\varphi] + \\ &+ \frac{1+\nu}{E} \sum_{n=0}^{\infty} A_n^* \left(\frac{r}{W} \right)^{n+1} [(n+4\nu-2) \cos n\varphi - (n+2) \cos(n+2)\varphi] \end{aligned} \quad (4.4)$$

$$\begin{aligned} \frac{v}{\sigma^* W} &= \frac{1+\nu}{E} \sum_{n=0}^{\infty} A_n \left(\frac{r}{W} \right)^{n+1/2} \frac{2n+3}{2n-1} [(n-\frac{1}{2}) \sin(n+\frac{3}{2})\varphi - (n-4\nu+\frac{7}{2}) \sin(n-\frac{1}{2})\varphi] + \\ &+ \frac{1+\nu}{E} \sum_{n=0}^{\infty} A_n^* \left(\frac{r}{W} \right)^{n+1} [(n+2) \sin(n+2)\varphi - (n-4\nu+4) \sin n\varphi] \end{aligned} \quad (4.5)$$

(ν =Poisson ratio), from which the needed Cartesian component results as

$$u_x = u \cos \varphi - \nu \sin \varphi \quad (4.6)$$

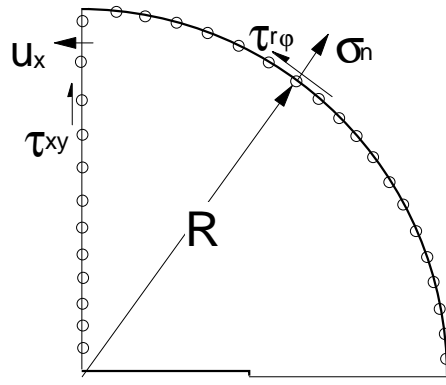


Fig. 4.1 Node selection and boundary conditions for an internally cracked disk.

In the special case of an internally cracked circular disk of radius R , the stresses at the boundaries are:

$$\sigma_n = \tau_{r\phi} = 0 \quad (4.7)$$

along the quarter circle. Along the perpendicular symmetry line, the boundary conditions are:

$$u_x = \text{const.} \rightarrow \frac{\partial u_x}{\partial y} = 0 \quad (4.8a)$$

$$\tau_{xy} = 0 \quad (4.8b)$$

About 100 coefficients for eq.(2) were determined from 600-800 stress and displacement equations at 400 nodes along the outer contour (symbolized by the circles in Fig. 4.1). For a selected number of $(N+1)$ collocation points, the related stress components (or displacements) are computed, and a system of $2(N+1)$ equations allows to determine up to $2(N+1)$ coefficients. The expenditure of computation can be reduced by the selection of a rather large number of edge points and by solving subsequently the then overdetermined system of equations using a least squares routine.

In the case of the edge-cracked rectangular plate of width W and height $2H$ (Fig. 4.2) the stresses at the border are

$$\sigma_x = 0, \tau_{xy} = 0 \quad \text{for } x = 0 \quad (4.9a)$$

$$\sigma_y = \sigma^*, \tau_{xy} = 0 \quad \text{for } y = H \quad (4.9b)$$

$$\sigma_x = 0, \tau_{xy} = 0 \quad \text{for } x = W \quad (4.9c)$$

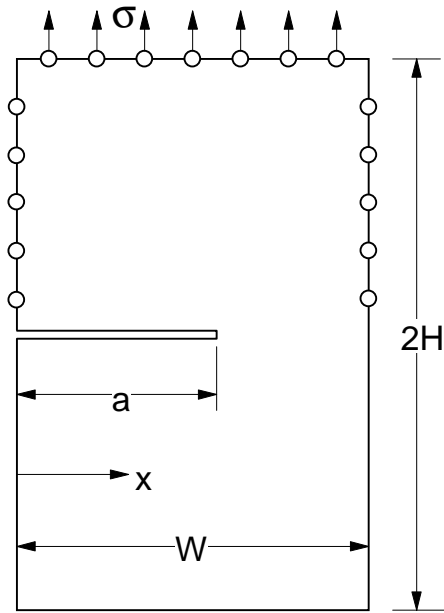


Fig. 4.2 Collocation points for the edge-cracked rectangular plate

and in the case of the Double-edge-cracked plate (Fig. 4.3) it holds

$$\sigma_x = 0, \tau_{xy} = 0 \quad \text{for } x = 0 \quad (4.10a)$$

$$\sigma_y = \sigma^*, \tau_{xy} = 0 \quad \text{for } y = H \quad (4.10b)$$

$$\frac{\partial u_x}{\partial y} = 0, \tau_{xy} = 0 \quad \text{for } x = W \quad (4.10c)$$

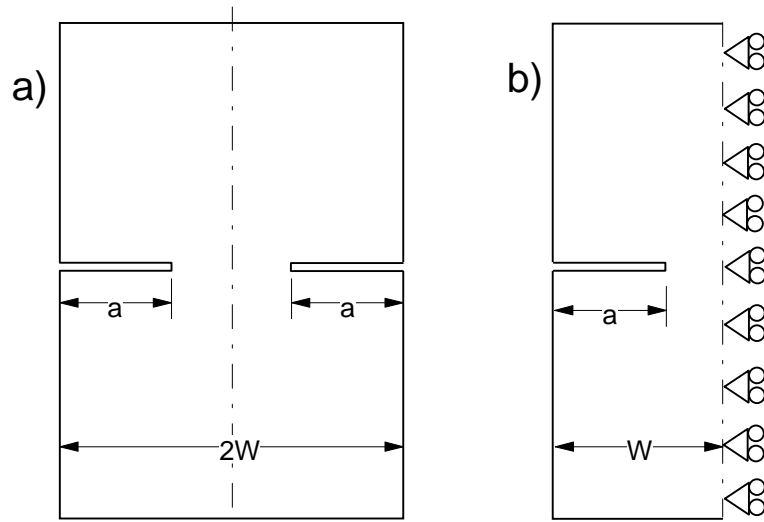


Fig. 4.3 Double-edge-cracked plate a) geometric data, b) half-specimen with symmetry boundary conditions.

4.2 Boundary Collocation procedure for point forces

The treatment of point forces at the crack face in case of a finite body is illustrated in the following sections for a circular disk with an internal crack loaded by a couple of forces at $x = y = 0$. In order to describe the crack-face loading by concentrated forces, we superimpose two loading cases. First, the singular crack-face loading is modelled by the centrally loaded crack in an infinite body described by the Westergaard stress function

$$Z = \frac{Pa}{\pi} \frac{1}{z\sqrt{z^2 - a^2}} \quad (4.11)$$

The stresses resulting from this stress function disappear only at infinite distances from the crack. In the finite body, consequently, the stress-free boundary condition is not fulfilled. To nullify the tractions at the outer boundaries, stresses resulting from the Airy stress function, eq.(2.2), are added which do not superimpose additional stresses at the crack faces. The basic principle used for such calculations, the principle of superposition, is illustrated in more detail in the Appendix.

The stresses caused by Z are

$$\sigma_x = \text{Re } Z - y \text{Im } Z' \quad (4.12)$$

$$\sigma_y = \text{Re } Z + y \text{Im } Z' \quad (4.13)$$

$$\tau_{xy} = -y \text{Re } Z' \quad (4.14)$$

with

$$Z' = \frac{dZ}{dz} = -\frac{Pa}{\pi} \frac{2z^2 - a^2}{z^2(z^2 - a^2)^{3/2}} \quad (4.15)$$

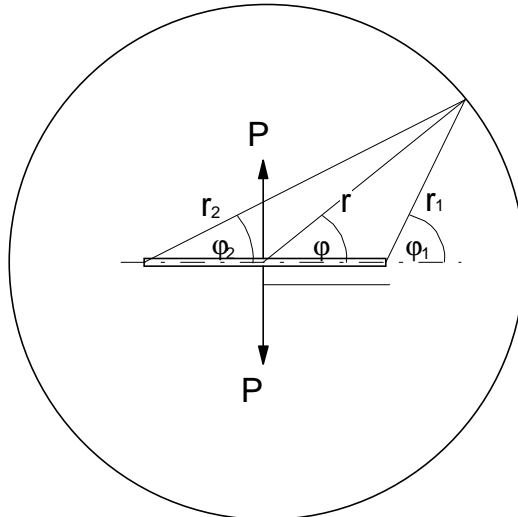


Fig.4.4 Coordinate system for the application of the Westergaard stress function to a finite component.

For practical use it is of advantage to introduce the coordinates shown in Fig.4.4. The following geometric relations hold

$$z = r \exp(i\varphi), \quad z - a = r_1 \exp(i\varphi_1), \quad z + a = r_2 \exp(i\varphi_2) \quad (4.16)$$

$$r = \sqrt{x^2 + y^2}, \quad \tan \varphi = y / x \quad (4.17a)$$

$$r_1 = \sqrt{(x - a)^2 + y^2}, \quad \tan \varphi_1 = y / (x - a) \quad (4.17b)$$

$$r_2 = \sqrt{(x + a)^2 + y^2}, \quad \tan \varphi_2 = y / (x + a) \quad (4.17c)$$

$$\operatorname{Re} Z = \frac{Pa}{\pi r \sqrt{r_1 r_2}} \cos(\varphi + \frac{1}{2} \varphi_1 + \frac{1}{2} \varphi_2) \quad (4.18a)$$

$$\operatorname{Im} Z = -\frac{Pa}{\pi r \sqrt{r_1 r_2}} \sin(\varphi + \frac{1}{2} \varphi_1 + \frac{1}{2} \varphi_2) \quad (4.18b)$$

$$\operatorname{Re} Z' = -\frac{Pa}{\pi} \left[\frac{2}{(r_1 r_2)^{3/2}} \cos \frac{3}{2}(\varphi_1 + \varphi_2) - \frac{a^2}{r^2 (r_1 r_2)^{3/2}} \cos(2\varphi + \frac{3}{2} \varphi_1 + \frac{3}{2} \varphi_2) \right] \quad (4.18c)$$

$$\operatorname{Im} Z' = \frac{Pa}{\pi} \left[\frac{2}{(r_1 r_2)^{3/2}} \sin \frac{3}{2}(\varphi_1 + \varphi_2) - \frac{a^2}{r^2 (r_1 r_2)^{3/2}} \sin(2\varphi + \frac{3}{2} \varphi_1 + \frac{3}{2} \varphi_2) \right] \quad (4.18d)$$

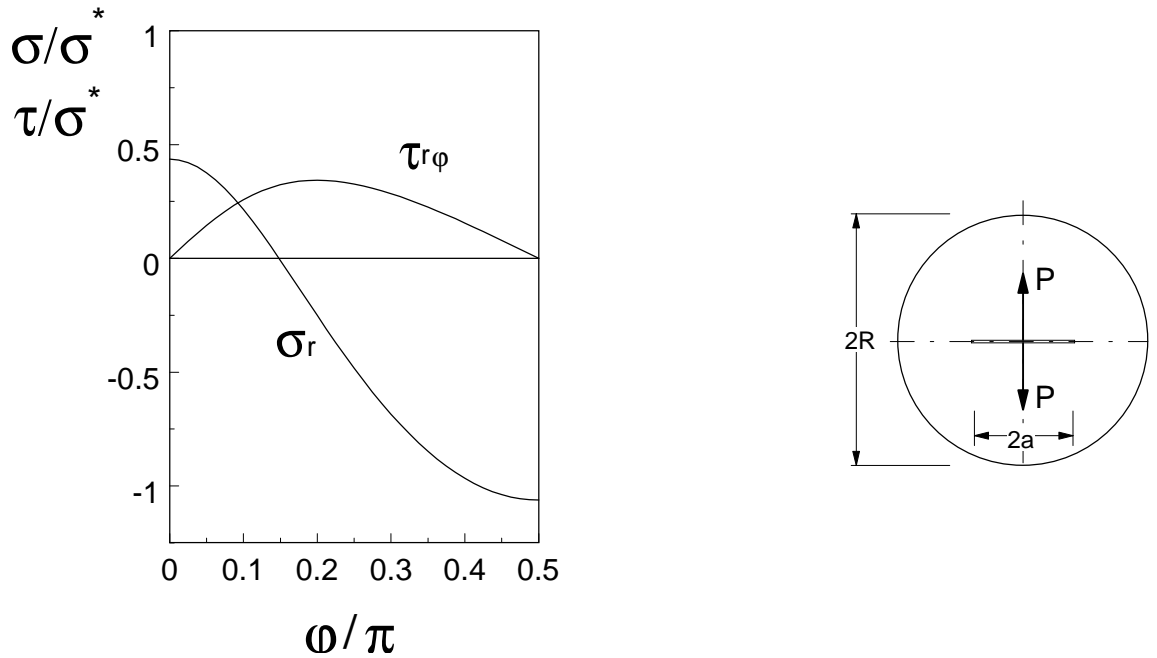


Fig.4.5 Normal and shear tractions created by the stress function (4.11) along the fictitious disk contour (for φ see Fig. 4.4), $\sigma^*=P/(\pi R)$.

The stress function Z provides no T-stress term as will be shown in 5.5.5. Nevertheless, the equilibrium tractions at the circumference act as a normal external load and may produce a T-stress. Radial and tangential stress components along the contour of the disk for a crack with $a/R=0.4$ are plotted in Fig.4.5.

5 Principle of superposition

The procedure necessary for the computations addressed in Section 4.2 is illustrated below. A disk geometry may be chosen. Figure 5.1 explains the principle of superposition for the case of T-stresses. Part a) shows a crack in an infinite body, loaded by a couple of forces P . The T-stress for this case is denoted as T_0 . First we compute the normal and shear stresses along a contour (dashed circle) which corresponds to the disk. We cut out the disk along this contour and apply normal and shear tractions at the free boundary which are identical with the stresses computed before (Fig. 5.1b).

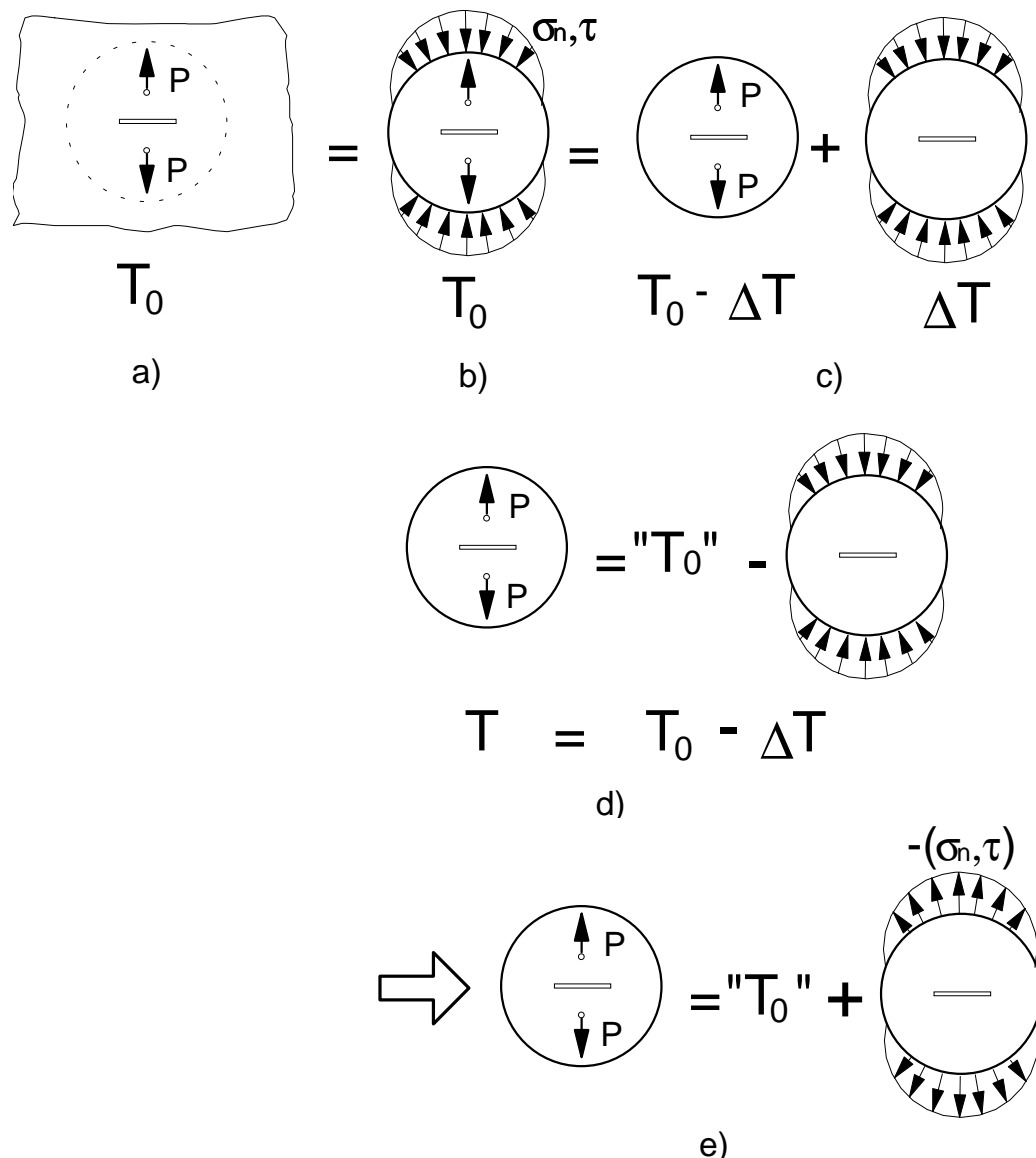


Fig. 5.1 Illustration of the principle of superposition for the computation of T-stresses for single forces.

The disk loaded by the combination of single forces and boundary tractions exhibit the same T-term T_0 . Next, we consider the situation b) to be the superposition of the two loading cases shown in part c), namely, the cracked disk loaded by the couple of forces (with T-stress $T-\Delta T$) and a cracked disk loaded by the boundary tractions, having the T-term ΔT . As represented by part d), the T-term of the cracked disk is the difference $T=T_0-\Delta T$. If the sign of the boundary tractions is changed, the equivalent relation is given by part e).

II RESULTS

The following sections contain numerical solutions for the T-stress term and the Green's function. The problems are subdivided in:

- Internally cracked components,
 - cracks in infinite bodies,
 - circular disk with internal crack,
 - rectangular plate with internal crack.
- Edge-cracked components,
 - rectangular plate with edge crack
 - edge-cracked circular disk,
 - cracks ahead of notches.
- Components with multiple edge cracks
 - double-edge-cracked rectangular plate,
 - double-edge-cracked circular disk,
 - array of deep edge cracks.

6 Crack in an infinite body

6.1 Couples of forces

The T-stress term resulting from a couple of symmetric point forces (see Fig. 6.1) can be derived from the Westergaard stress function [16] which for this special case reads

$$Z = \frac{2P}{\pi} \frac{\sqrt{a^2 - x^2}}{(z^2 - x^2)\sqrt{1 - (a/z)^2}} \quad (6.1)$$

(note that eq.(3.5) is the limit of this relation for $x \rightarrow a$). The real part of (6.1) gives the x-stress component for $y=0$

$$\sigma_x|_{y=0} = \text{Re}\{Z\} = \frac{2P}{\pi} \frac{\sqrt{a^2 - x^2} x'}{(x'^2 - x^2)\sqrt{x'^2 - a^2}} \quad (6.2)$$

Its singular part

$$\sigma_{x,\text{sing}}|_{y=0} = \frac{2P}{\pi} \frac{\sqrt{a/2}}{\sqrt{a^2 - x^2} \sqrt{x' - a}} \quad (6.3)$$

provides the well-known stress intensity factor solution

$$K = \lim_{x' \rightarrow a} \sqrt{2\pi(x' - a)} \sigma_x = \sqrt{\frac{a}{\pi}} \frac{2P}{\sqrt{a^2 - x^2}} \quad (6.4)$$

Then, the regular stress term reads

$$\sigma_{x,\text{reg}}|_{y=0} = \frac{2P}{\pi} \frac{(a^2 - x^2)x' - \sqrt{a/2}(x'^2 - x^2)\sqrt{x' + a}}{(x'^2 - x^2)\sqrt{x'^2 - a^2} \sqrt{a^2 - x^2}} \quad (6.5)$$

and for the T-stress term it results

$$T = \lim_{x' \rightarrow a} \sigma_{x,\text{reg}} = \begin{cases} 0 & \text{for } x < a \\ \infty & \text{for } x = a \end{cases} \quad (6.6)$$

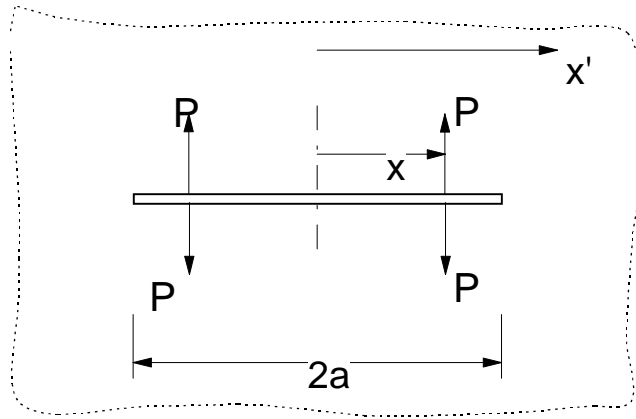


Fig. 6.1 Crack in an infinite body loaded by symmetric couples of forces.

6.2 Constant crack-face loading

In the case of a constant crack-face pressure $p = \text{const.}$ (Fig. 6.2), the stress function reads

$$Z = p \left[\frac{z}{\sqrt{z^2 - a^2}} - 1 \right] \quad (6.7)$$

resulting in the x-stress of

$$\sigma_x|_{y=0} = p \left[\frac{x'}{\sqrt{x'^2 - a^2}} - 1 \right] \quad (6.8)$$

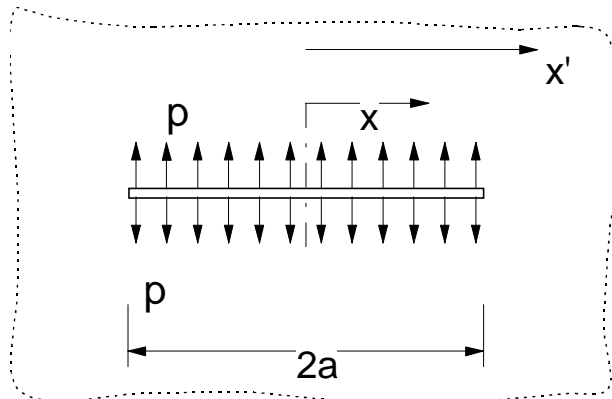


Fig. 6.2 Crack in an infinite body under constant crack-face pressure.

The T-stress term results as

$$T = -p \quad (6.9)$$

as found for the small-scale solution (3.18).

7 Circular disk with internal crack

7.1 Constant internal pressure

The crack under constant internal pressure (Fig. 7.1) has been analyzed with the Boundary Collocation method. T-stress data are shown in Fig. 7.2 and Table 7.1.

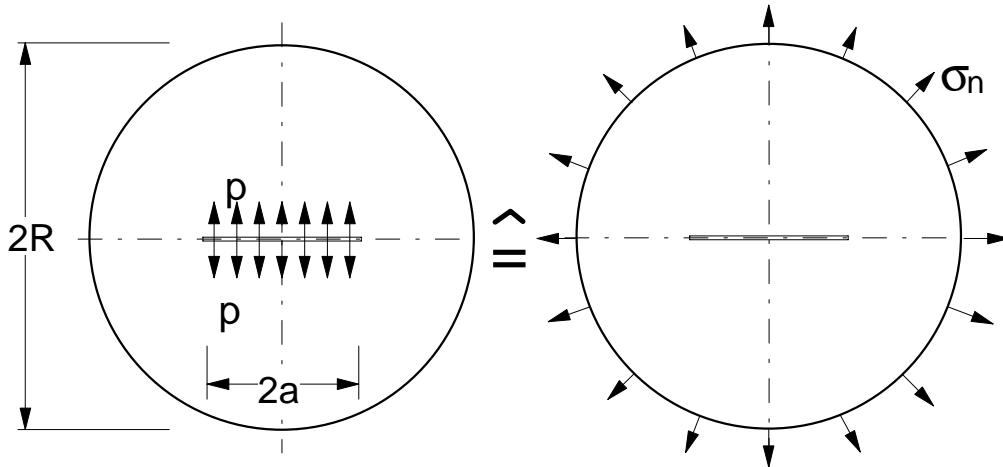


Fig. 7.1 Circular disk with internal crack under constant pressure p and equivalent problem of disk loading by normal tractions at the circumference.

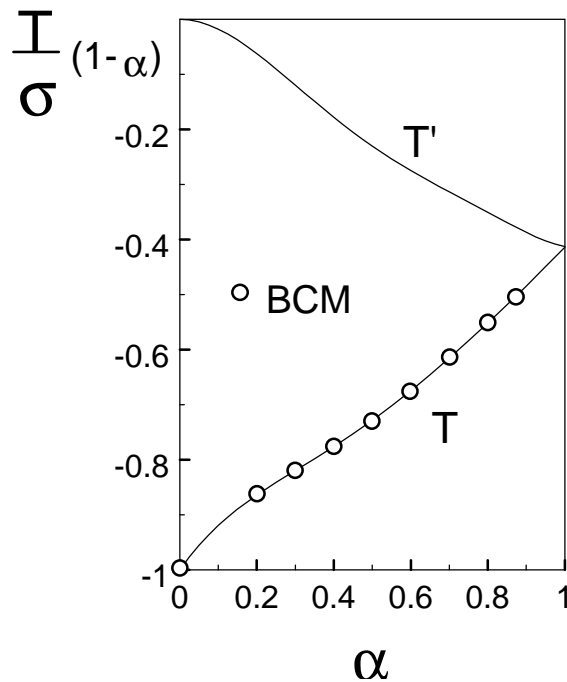


Fig. 7.2 T-stress and geometric function F for the stress intensity factor for an internal crack in a circular disk.

$\alpha = a/R$	$T/\sigma \cdot (1-\alpha)$	$T'/\sigma \cdot (1-\alpha)$	$\beta \cdot (1-\alpha)^{1/2}$
0	-1.00	0.000	-1.00
0.1	-0.919	-0.019	-0.952
0.2	-0.864	-0.064	-0.909
0.3	-0.820	-0.120	-0.862
0.4	-0.776	-0.176	-0.807
0.5	-0.728	-0.228	-0.744
0.6	-0.675	-0.275	-0.676
0.7	-0.615	-0.315	-0.608
0.8	-0.552	-0.352	-0.550
0.9	-0.485	-0.385	-0.509
1.0	-0.413	-0.413	-0.50

Table 7.1 T-stress for an internally cracked circular disk with constant crack-face pressure (value T for $\alpha = 1$ extrapolated); for T and T' see eqs.(2.7) and (2.8).

The T-values in Table 7.1 were extrapolated to $\alpha = 1$. Within the numerical accuracy of the extrapolation, the limit values are

$$\lim_{\alpha \rightarrow 1} T / \sigma * (1 - \alpha) = \lim_{\alpha \rightarrow 1} T' / \sigma * (1 - \alpha) \cong -0.413 = -\frac{1}{\sqrt{\pi^2 - 4}} \quad (7.1)$$

and for the biaxiality ratio

$$\lim_{\alpha \rightarrow 1} \beta \sqrt{1 - \alpha} \cong \frac{1}{2} \quad (7.2)$$

The T-stress terms can be approximated by

$$T / \sigma = \frac{-1 + \alpha - 2.34\alpha^2 + 4.27\alpha^3 - 3.326\alpha^4 + 0.9824\alpha^5}{1 - \alpha} \quad (7.3)$$

$$T' / \sigma = \frac{-2.34\alpha^2 + 4.27\alpha^3 - 3.326\alpha^4 + 0.9824\alpha^5}{1 - \alpha} \quad (7.4)$$

The stress intensity factor solution (found in the BCM-computations) is in good agreement with the geometric function [9]

$$F = \frac{K}{\sigma_n \sqrt{\pi a}} \frac{1 - 0.5\alpha + 1.6873\alpha^2 - 2.671\alpha^3 + 3.2027\alpha^4 - 1.8935\alpha^5}{\sqrt{1 - \alpha}}. \quad (7.5)$$

7.2 Disk partially loaded by normal tractions

A partially loaded disk is shown in Fig.7.3a. Constant normal tractions σ_n are applied at the circumference within an angle of 2γ .

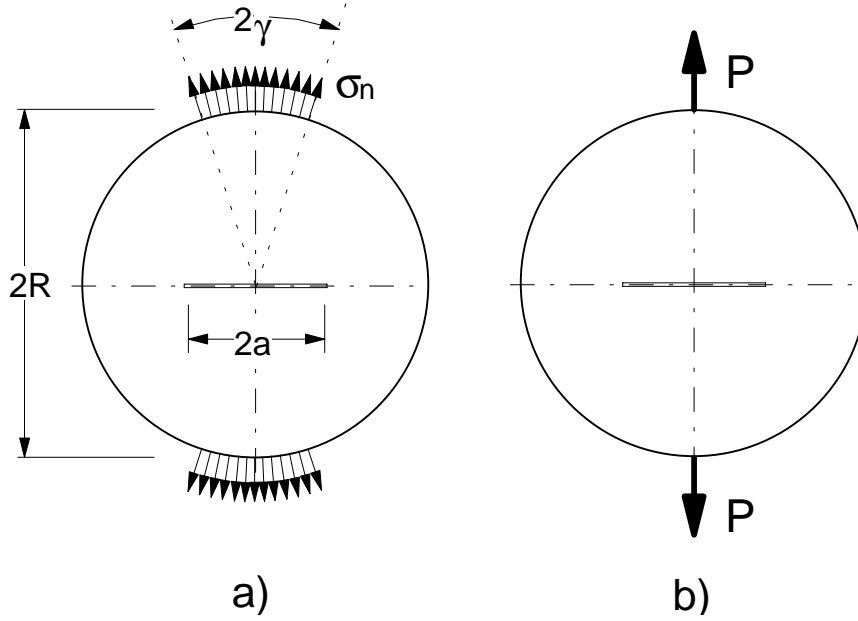


Fig. 7.3 a) partially loaded disk, b) diametral loading by a couple of forces.

The total force in y-direction results from

$$P_y = 2\sigma_n \int_0^\gamma R \cos \gamma' d\gamma' = 2\sigma_n R \sin \gamma \quad (7.6)$$

The x-stress term T' , normalised to σ^* , is shown in Fig. 7.4.

From the limit case $\gamma \rightarrow 0$, the solutions for concentrated forces (see Fig. 7.3b) are obtained as represented in Fig. 7.5.

The T-stress T' can be fitted by

$$\frac{T'}{\sigma^*} = \frac{-4(1-\alpha) + 7.6777\alpha^2 - 16.0169\alpha^3 + 8.7994\alpha^4 - 1.10849\alpha^5}{1-\alpha} \quad (7.7)$$

Since the stresses in the uncracked disk under diametral loading by the couple of forces P are

$$\frac{\sigma_y}{\sigma^*} = \frac{4}{(1+\xi^2)^2} - 1, \quad \frac{\sigma_x}{\sigma^*} = -1 + \frac{4\xi^2}{(1+\xi^2)^2}, \quad \xi = x/R \quad (7.8)$$

with σ^* defined as

$$\sigma^* = \frac{P_y}{\pi R}, \quad (7.9)$$

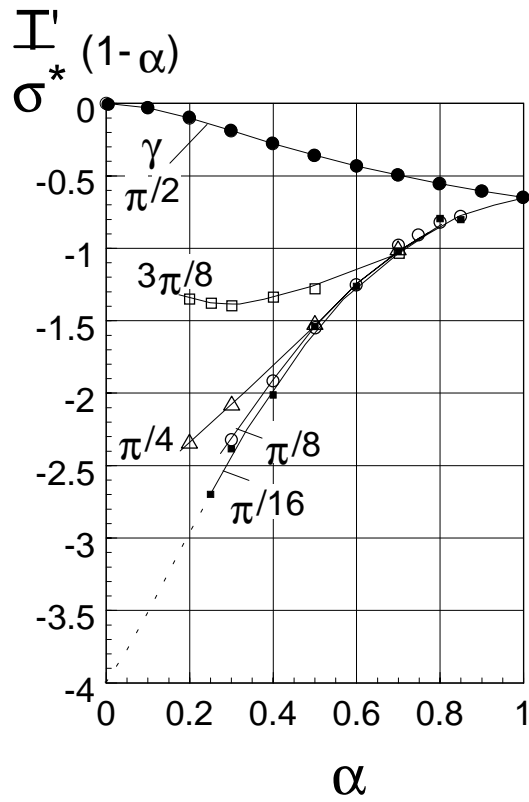


Fig. 7.4 T-stress for a circular disk, partially loaded over an angle of 2γ (see Fig. 7.3a).

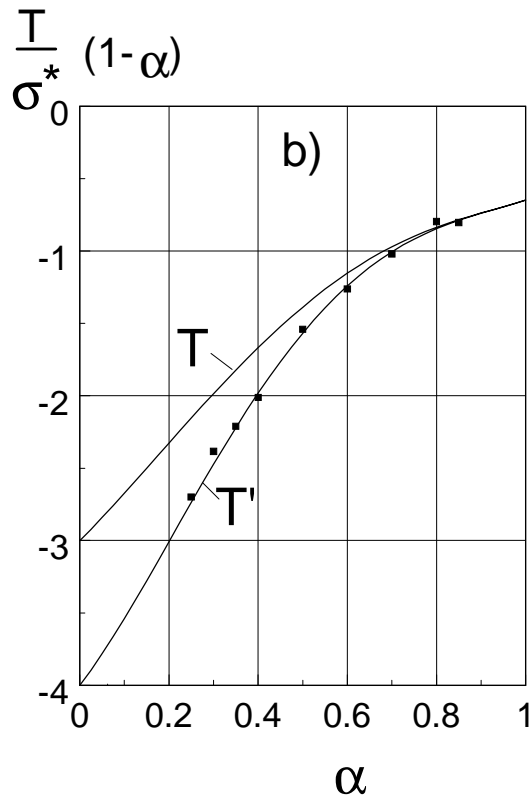


Fig. 7.5 T-stress for a circular disk loaded diametrically by concentrated forces (Fig. 7.3b). T-stress results including partially distributed stresses with an angle of $\gamma=\pi/16$ (squares) and exact limit cases for $\alpha=0$.

T can be computed from T'

$$\frac{T}{\sigma^*} = \frac{-3(1-\alpha) + 7.6777\alpha^2 - 16.0169\alpha^3 + 8.7994\alpha^4 - 1.10849\alpha^5}{1-\alpha} - \frac{4\alpha^2}{(1+\alpha^2)^2} \quad (7.10)$$

or expressed by a fit relation

$$\frac{T}{\sigma^*} \cong \frac{-3(1-\alpha) + 2.8996\alpha^2 - 6.1759\alpha^3 + 2.5438\alpha^4 + 0.0841\alpha^5}{1-\alpha} \quad (7.11)$$

In this case, the limit values are (at least in very good approximation)

$$\lim_{\alpha \rightarrow 1} T / \sigma^* (1-\alpha) = \lim_{\alpha \rightarrow 1} T' / \sigma^* (1-\alpha) \cong -0.648 \cong -\frac{\pi}{2\sqrt{\pi^2 - 4}} \quad (7.12)$$

7.3 Central point force on the crack face

A centrally cracked circular disk, loaded by a couple of forces at the crack center, is shown in Fig.7.6. For it, the T-stress was calculated by Boundary Collocation computations.

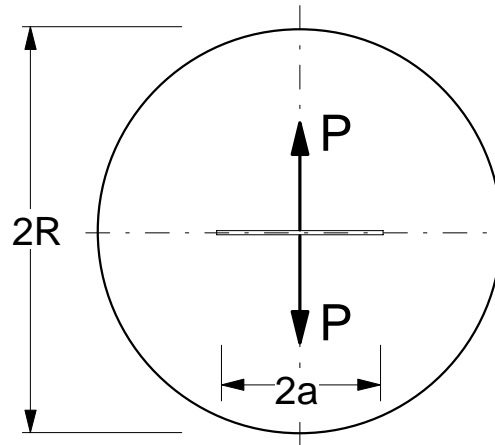


Fig. 7.6 Circular disk with a couple of forces acting on the crack faces.

The T-stress data obtained with the BCM-method according to Section 4.2 are plotted in Fig. 7.7 as squares. Together with the limit value (7.12) the numerically found T-values were fitted by the polynomial

$$\frac{T}{\sigma^*} = \frac{-4.1971\alpha + 5.4661\alpha^2 - 1.1497\alpha^3 - 0.7677\alpha^4}{1-\alpha} \quad (7.13)$$

This relation is introduced into Fig. 7.7 as the solid line.

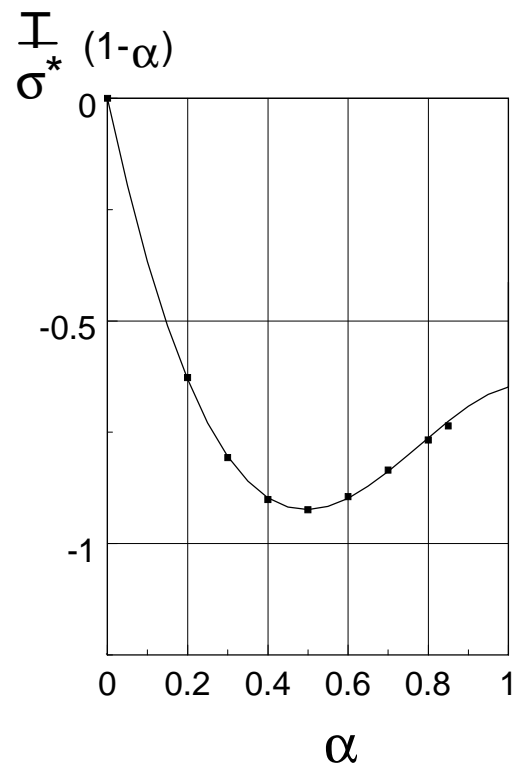


Fig. 7.7 T-stress for an internally cracked circular disk with a couple of forces acting in the crack center on the crack faces. Symbols: Numerical results, solid line: fitting curve.

8 Estimation of T-terms with a Green's function

8.1 Green's function with one regular term

In order to estimate T-stresses, an approximate Green's function according to eqs.(3.25) and (3.26) may be applied. A Green's function with only one term was derived according to Section 3.2.3 using the case of constant crack-face pressure σ_0 as the reference loading case. In this rough approximation the T-term results as

$$T = C \int_0^a (1 - x^2 / a^2) \sigma_y(x) dx - \sigma_y|_{x=a}, \quad C = \frac{3}{2a} \left(1 + \frac{T_\sigma}{\sigma_0} \right) \quad (8.1)$$

This section now deals with a check of the accuracy of the approximate Green's function by comparing the results of the set-up (3.25) with T-stress solutions found by application of the Boundary Collocation procedure.

First, the case of concentrated forces at $x=0$ (see Fig. 7.6) is considered. The couple of central forces reads in terms of the Dirac δ -function ($B=1$)

$$\sigma_y(x) = \frac{P}{2} \delta(x) \quad (8.2)$$

Introducing this and (7.4) into (8.1) leads to

$$T \approx \frac{3P}{4a} \left(1 + \frac{T_\sigma}{\sigma_0} \right) \quad (8.3)$$

$$\frac{T}{\sigma^*} \approx \frac{3\pi}{4} \frac{-2.34\alpha + 4.27\alpha^2 - 3.326\alpha^3 + 0.9824\alpha^4}{1-\alpha}, \quad \sigma^* = \frac{P}{R\pi} \quad (8.4)$$

The result is plotted in Fig. 8.1.

As a second example, the diametral tension test is considered (see Fig. 7.3b). Introducing the stress distribution for a diametral tension test, eq.(7.8), into (8.1) yields, after numerical integration, the T-stress shown in Fig. 8.2.

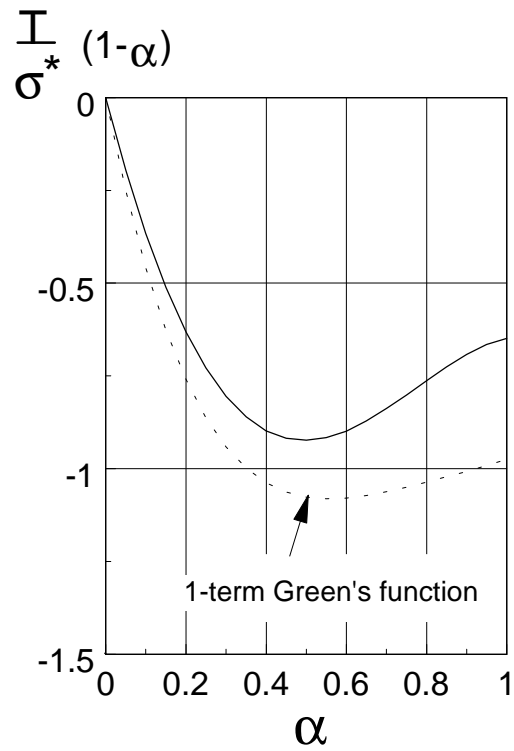


Fig. 8.1 T-stresses for an internally cracked circular disk, loaded by a couple of forces at the crack faces (see Fig. 7.6) estimated with a 1-term Green's function (dashed curve) compared with results from BCM-computations (solid curve).

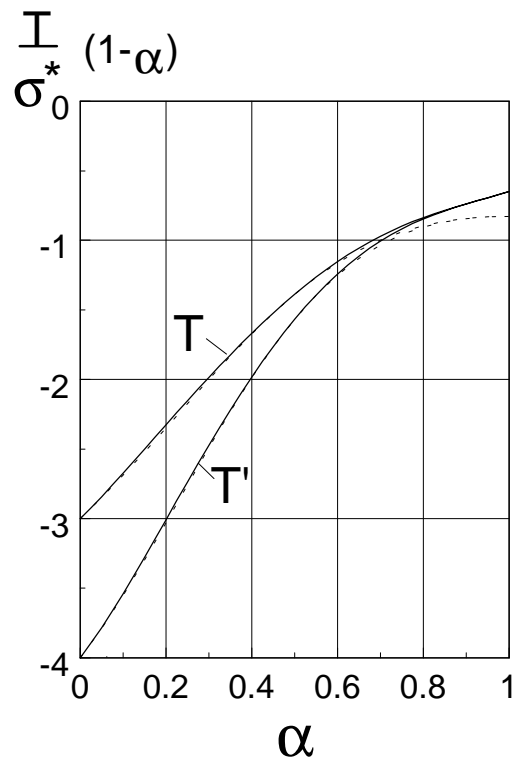


Fig. 8.2 T-stresses for an internally cracked circular disk, loaded by a couple of diametral forces at the free boundary (see Fig. 7.3b) estimated with a 1-term Green's function (dashed curve) compared with results from BCM-computations (solid curve).

From these two examples we can conclude for this first degree of approximation that the application to continuously distributed stresses gives significantly better results than the application to strongly non-homogeneous stresses as in the case of single forces at the crack faces. The reason for this behaviour is the fact that in the reference loading case (constant crack-face pressure) the load was also distributed homogeneously. In both cases the deviations increase with increasing relative crack size α . This makes evident that the Green's function needs higher order terms for larger α .

8.2 Green's function with two regular terms

In order to improve the Green's function, the next regular term is added. Consequently, the Green's function expansion reads

$$t = t_0 + C_1(1 - x^2 / a^2) + C_2(1 - x^2 / a^2)^2 \quad (8.5)$$

As a second reference loading case we now use the solution T_P for the internally cracked disk with a pair of single forces P at the crack center (see Fig. 7.6).

Introducing the two reference stresses

$$\sigma_1 = \text{const.} \quad \sigma_2 = \frac{P}{2} \delta(x) \quad (8.6)$$

into eq.(3.1) and carrying out the integration provides a system of two equations

$$T_1 / \sigma_1 = -1 + \frac{2a}{3} C_1 + \frac{8a}{15} C_2 \quad (8.7a)$$

$$T_2 / \sigma^* = \frac{\pi R}{2} C_1 + \frac{\pi R}{2} C_2 \quad (8.7b)$$

($\sigma^* = P / (R\pi)$) from which the coefficients result as

$$C_1 = \frac{15}{2a} \left(1 + \frac{T_1}{\sigma_1} \right) - 8 \frac{T_2}{R\pi\sigma^*} \quad (8.8a)$$

$$C_2 = -\frac{15}{2a} \left(1 + \frac{T_1}{\sigma_1} \right) + 10 \frac{T_2}{R\pi\sigma^*} \quad (8.8b)$$

or by

$$C_1 = \frac{1}{R} \frac{-6.8622 \alpha + 18.1057 \alpha^2 - 22.0173 \alpha^3 + 9.3229 \alpha^4}{1 - \alpha} \quad (8.8c)$$

$$C_2 = \frac{1}{R} \frac{4.1902\alpha - 14.626\alpha^2 + 21.2854\alpha^3 - 9.8117\alpha^4}{1-\alpha} \quad (8.8d)$$

With the improved Green's function the diametral tension specimen was computed again using eq.(7.8). The result is plotted in Fig. 8.3. It becomes obvious that in this approximation the agreement is significantly better for large α .

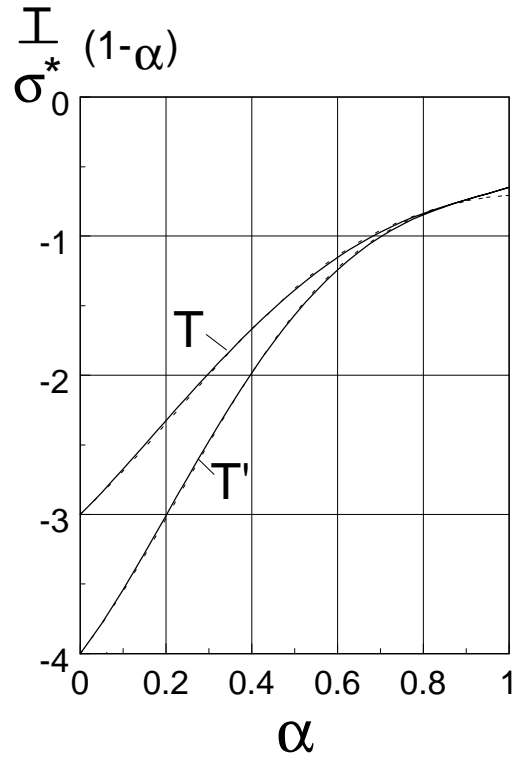


Fig. 8.3 T-stresses for an internally cracked circular disk, loaded by a couple of diametral forces at the free boundary (see Fig. 7.3b) estimated with a 2-terms Green's function (dashed curve) compared with results from BCM-computations (solid curve).

9 Rectangular plate with internal crack

The geometric data of the rectangular plate with an internal crack are illustrated in Fig.9.1.

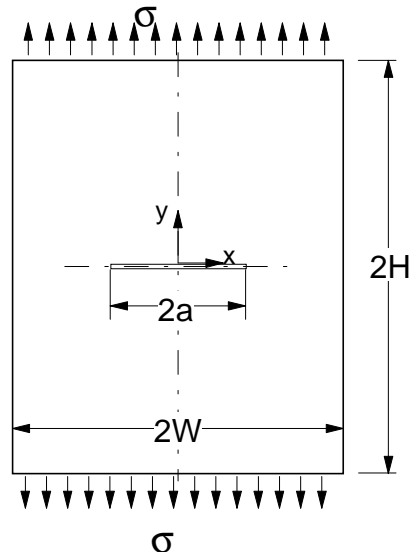


Fig. 9.1 Rectangular plate with a central internal crack (geometric data).

9.1 T-stress for pure tensile load

The plate under uniaxial load (tensile stresses at the ends $y = \pm H$) shows no σ_x -component in the uncracked structure. Consequently, the quantities T and T' are identical. T-stress results obtained by BCM-computations are shown in Fig. 9.2a and entered into Table 9.1.

$\alpha = a/W$	$H/W=0.35$	0.50	0.75	1.00	1.25
0	-1.0	-1.0	-1.0	-1.0	-1.0
0.1	-0.97	-0.96	-0.92	-0.91	-0.9
0.2	-0.95	-0.92	-0.88	-0.86	-0.83
0.3	-0.766	-0.855	-0.85	-0.809	-0.777
0.4	-0.455	-0.745	-0.805	-0.756	-0.716
0.5	-0.110	-0.616	-0.738	-0.692	-0.656
0.6	0.145	-0.502	-0.647	-0.620	-0.596
0.7	0.215	-0.400	-0.543	-0.55	-0.53
0.8	0.13	-0.291	-0.45	-0.46	-0.47
0.9	-0.10	-0.25	-0.38	-0.41	-0.43
1.0	-0.413	-0.413	-0.413	-0.413	-0.413

Table 9.1 T-stress term, normalized as $T/\sigma(1-\alpha)$, for different crack and plate geometries.

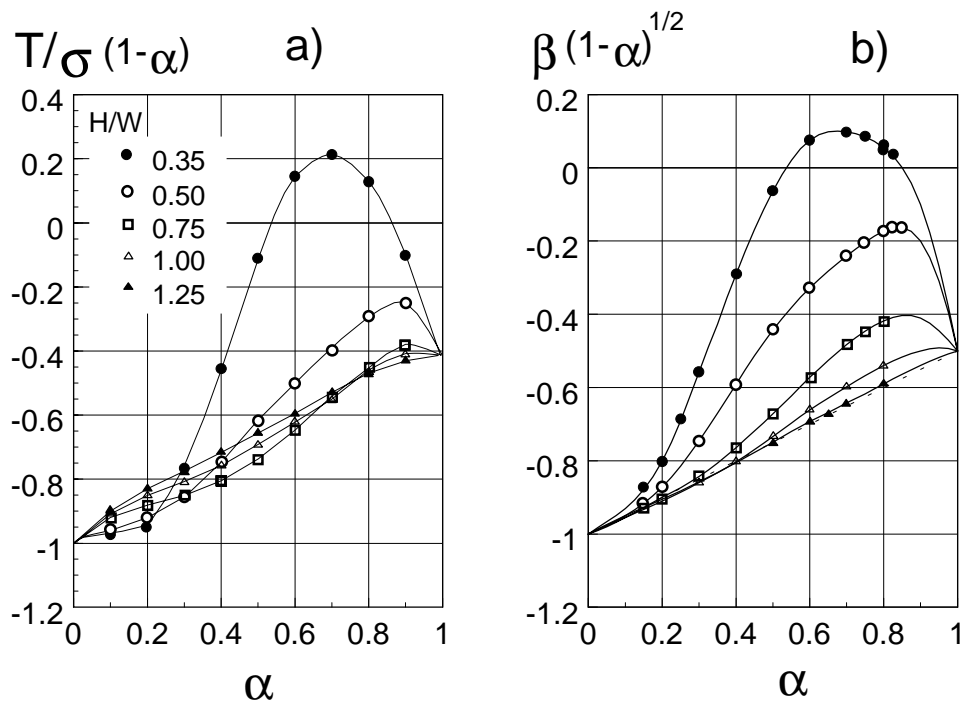


Fig.9.2 Internal crack in rectangular plate, a) T-stress, b) biaxiality ratio.

The biaxiality ratio, defined by eq.(2.9), is plotted in Fig. 9.2b and additionally given in Table 9.2.

For a long plate ($H/W > 1.5$) the biaxiality ratio β can be expressed by

$$\beta \cong -\frac{1-0.5\alpha}{\sqrt{1-\alpha}} \quad (9.1)$$

$\alpha = a/W$	$H/W=0.35$	0.50	0.75	1.00	1.25
0	-1.0	-1.0	-1.0	-1.0	-1.0
0.1	-0.93	-0.95	-0.955	-0.955	-0.95
0.2	-0.801	-0.872	-0.90	-0.91	-0.905
0.3	-0.558	-0.746	-0.843	-0.860	-0.858
0.4	-0.291	-0.591	-0.764	-0.803	-0.805
0.5	-0.063	-0.443	-0.672	-0.734	-0.749
0.6	0.075	-0.328	-0.573	-0.661	-0.693
0.7	0.098	-0.241	-0.483	-0.598	-0.645
0.8	0.055	-0.173	-0.418	-0.54	-0.59
0.9	-0.1	-0.2	-0.41	0.5	-0.54
1.0	-0.5	-0.5	-0.5	-0.5	-0.5

Table 9.2 Biaxiality ratio, normalized as $\beta(1-\alpha)^{1/2}$, for different crack and plate geometries.

10 Edge-cracked rectangular plate

10.1 Rectangular plate under tension

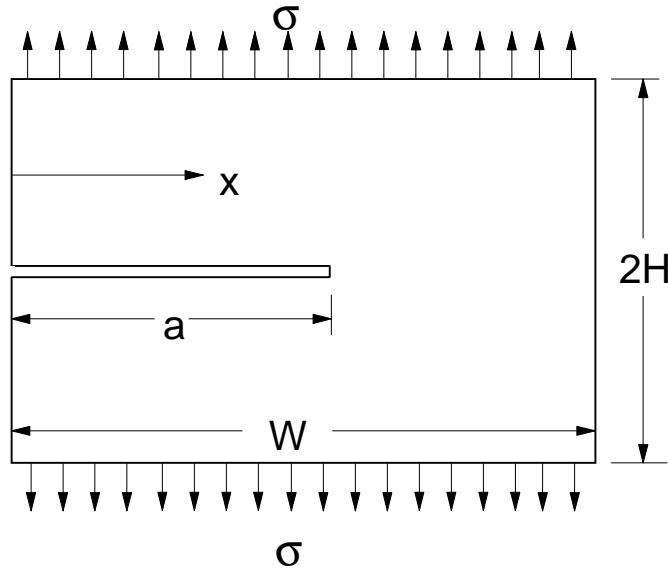


Fig. 10.1 Edge-cracked rectangular plate under tensile loading.

$\alpha = a/W$	$H/W=1.5$	0.75	0.50	0.40	0.30	0.25
0	-0.526	-0.526	-0.526	-0.526	-0.526	-0.526
0.1	-0.452	-0.452	-0.444	-0.432	-0.416	-0.400
0.2	-0.374	-0.373	-0.334	-0.270	-0.084	0.143
0.3	-0.299	-0.282	-0.148	0.030	0.449	0.890
0.4	-0.208	-0.175	0.040	0.310	0.912	1.526
0.5	-0.106	-0.070	0.167	0.473	1.165	1.858
0.6	0.006	0.032	0.220	0.490	1.142	1.812
0.7	0.122	0.134	0.234	0.404	0.869	1.387
0.8	0.232	0.240	0.268	0.324	0.524	0.760
0.9	0.352	0.356	0.364	0.372	0.376	0.380
1.0	0.474	0.474	0.474	0.474	0.474	0.474

Table 10.1a T-stress for a plate under tension $T/\sigma \cdot (1-a/W)^2$.

For a long plate ($H/W \geq 1.5$) the T-stress is

$$\frac{T}{\sigma} = \frac{-0.526 + 0.641\alpha + 0.2049\alpha^2 + 0.755\alpha^3 - 0.7974\alpha^4 + 0.1966\alpha^5}{(1-\alpha)^2} \quad (10.1a)$$

The related biaxiality ratio is fitted by

$$\beta = \frac{-0.469 + 0.1414\alpha + 1.433\alpha^2 + 0.0777\alpha^3 - 1.6195\alpha^4 + 0.859\alpha^5}{\sqrt{1-\alpha}} \quad (10.1b)$$

$\alpha = a/W$	H/W=1.5	0.75	0.50	0.40	0.30	0.25
0	-0.469	-0.469	-0.469	-0.469	-0.469	-0.469
0.1	-0.444	-0.444	-0.429	-0.406	-0.363	-0.322
0.2	-0.381	-0.379	-0.314	-0.232	-0.062	0.087
0.3	-0.307	-0.288	-0.137	0.024	0.302	0.516
0.4	-0.212	-0.177	0.037	0.256	0.605	0.856
0.5	-0.106	-0.069	0.157	0.406	0.814	1.091
0.6	0.006	0.031	0.209	0.443	0.885	1.204
0.7	0.117	0.128	0.223	0.377	0.755	1.092
0.8	0.217	0.226	0.252	0.305	0.480	0.678
0.9	0.321	0.325	0.332	0.341	0.343	0.346
1.0	0.423	0.423	0.423	0.423	0.423	0.423

Table 10.1b Biaxiality ratio β in the form $\beta(1-a/W)^{1/2}$.

10.2 Rectangular plate under bending load

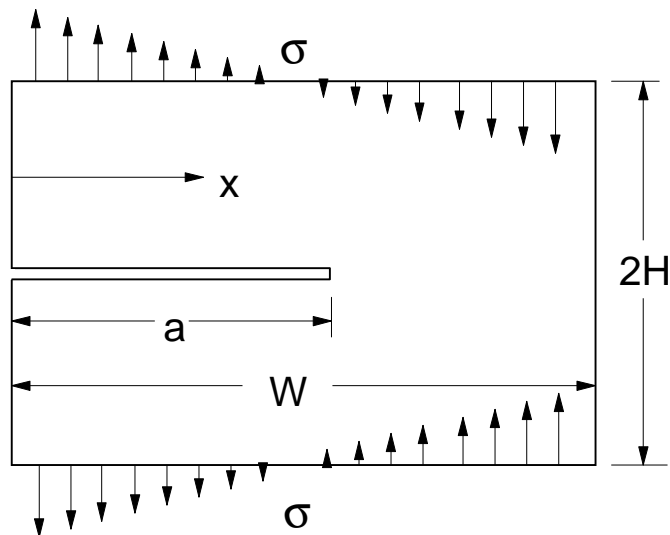


Fig. 10.2 Edge-cracked rectangular plate under bending loading.

For a long plate ($H/W \geq 1.5$) the T-stress is

$$\frac{T}{\sigma_b} = \frac{-0.526 + 2.481\alpha - 3.553\alpha^2 + 2.6384\alpha^3 - 0.9276\alpha^4}{(1-\alpha)^2} \quad (10.2a)$$

with the bending stress σ_b defined by

$$\sigma(x) = \sigma_b(1 - 2x/W) \quad (10.3)$$

The related biaxiality ratio is fitted by

$$\beta = \frac{-0.469 + 1.0485\alpha + 2.595\alpha^2 - 6.666\alpha^3 + 6.271\alpha^4 - 2.478\alpha^5}{\sqrt{1-\alpha}} \quad (10.2b)$$

$\alpha = a/W$	H/W=1.5	0.75	0.50	0.40	0.30	0.25
0	-0.526	-0.526	-0.526	-0.526	-0.526	-0.526
0.2	-0.150	-0.148	-0.114	-0.061	0.099	0.292
0.3	-0.039	-0.024	0.080	0.222	0.559	0.920
0.4	0.044	0.067	0.224	0.424	0.873	1.333
0.5	0.099	0.124	0.283	0.493	0.964	1.439
0.6	0.133	0.150	0.269	0.438	0.840	1.251
0.7	0.151	0.158	0.217	0.314	0.574	0.857
0.8	0.158	0.158	0.174	0.204	0.302	0.426
0.9	0.140	0.142	0.150	0.162	0.169	0.186
1.0	0.113	0.113	0.113	0.113	0.113	0.113

Table 10.2a T-stress for a plate under bending $T/\sigma \cdot (1-a/W)^2$.

$\alpha = a/W$	H/W=1.5	1.00	0.75	0.50	0.40	0.30
0	-0.469	-0.469	-0.469	-0.469	-0.469	-0.469
0.2	-0.198	-0.20	-0.194	-0.138	-0.067	0.091
0.3	-0.059	-0.057	-0.036	0.107	0.262	0.527
0.4	0.075	0.077	0.113	0.341	0.565	0.907
0.5	0.187	0.191	0.233	0.495	0.772	1.189
0.6	0.275	0.278	0.326	0.536	0.816	1.305
0.7	0.337	0.338	0.353	0.481	0.680	1.135
0.8	0.376	0.375	0.378	0.416	0.487	0.711
1.0	0.302	0.302	0.302	0.302	0.302	0.302

Table 10.2b Biaxiality ratio β in the form $\beta(1-a/W)^{1/2}$.

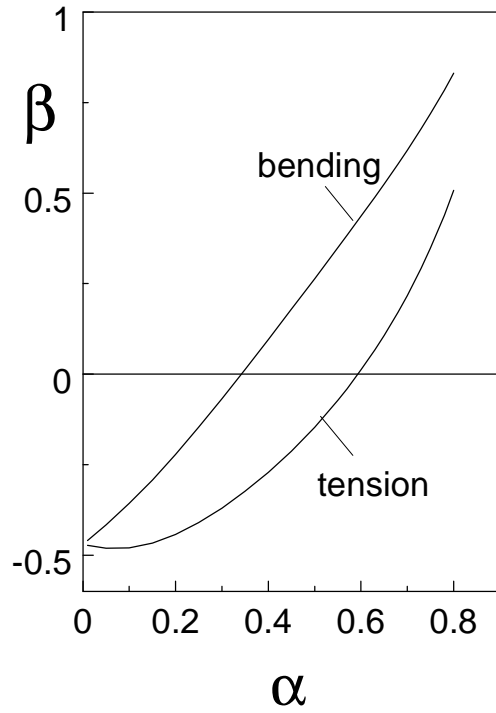


Fig. 10.3 T-stress for an edge-cracked plate or bar in tension and bending

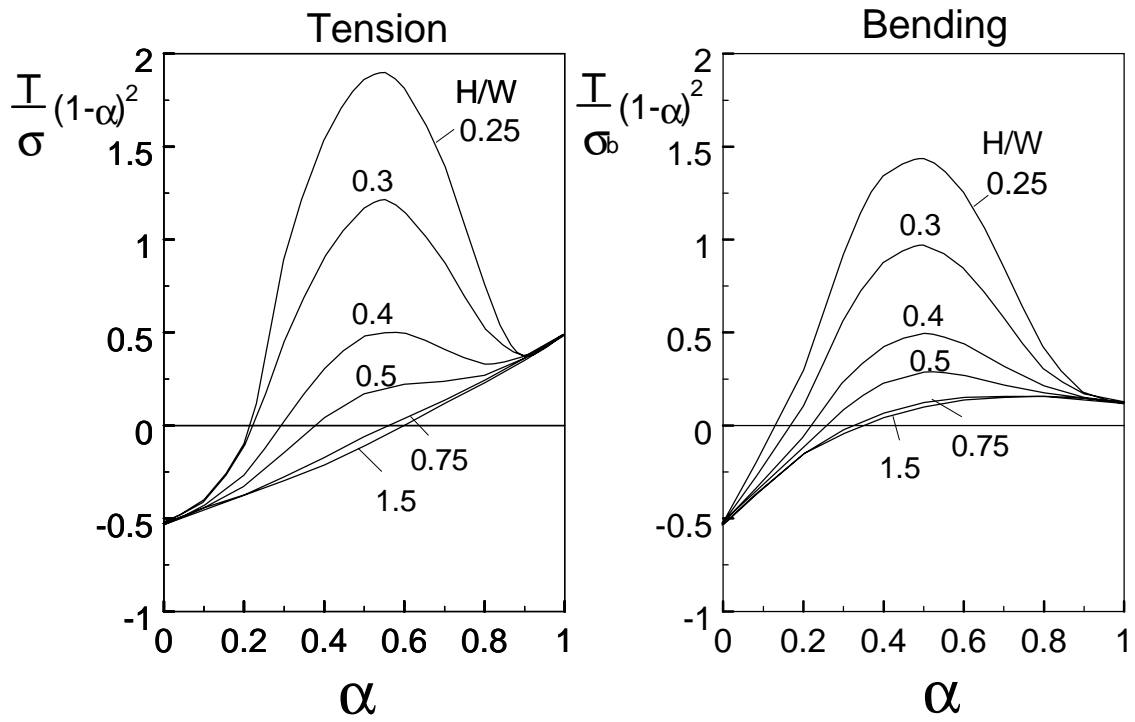


Fig. 10.4 T-stress under tensile and bending loadings.

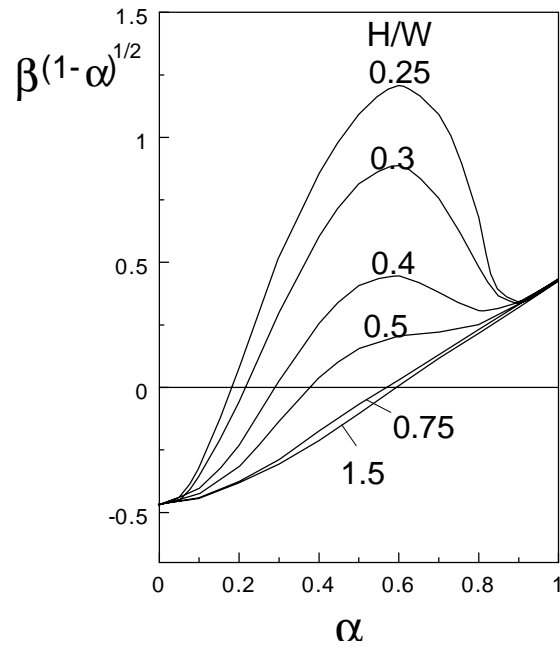


Fig. 10.5 Biaxiality ratio in the form $\beta(1-\alpha)^{1/2}$ for tension.

Green's function

$$t(x) = t_0 + C_1(1 - x/a) + C_2(1 - x/a)^2 \quad (10.4)$$

or

$$T = -\sigma_y \Big|_{x=a} + C_1 \int_0^a \sigma_y(x)(1 - x/a) dx + C_2 \int_0^a \sigma_y(x)(1 - x/a)^2 dx \quad (10.5)$$

with the coefficients C_1 and C_2 given in the following tables.

$\alpha = a/W$	H/W=1.5	0.75	0.50	0.40	0.30
0.2	2.531	2.015	2.53	4.78	8.16
0.3	1.456	1.306	4.00	6.53	11.74
0.4	1.167	1.792	4.93	8.33	15.13
0.5	1.728	2.112	5.71	9.46	18.67
0.6	3.167	3.417	6.04	10.21	21.60
0.7	6.204	6.422	8.05	11.73	23.31

Table 10.3 Coefficient $C_1 \cdot W$ for the Green's function, eq.(10.4).

$\alpha = a/W$	H/W=1.5	0.75	0.50	0.40	0.30
0.2	2.438	3.234	3.37	1.50	0.80
0.3	1.714	2.286	0.980	0.82	1.55
0.4	1.417	1.167	0.925	1.46	3.81
0.5	0.864	1.152	1.44	3.17	5.95
0.6	0.437	0.875	2.81	5.00	8.28
0.7	0.789	1.034	3.35	5.93	10.71

Table 10.4 Coefficient $C_2 \cdot W$ for the Green's function, eq.(10.4).

10.3 Edge-cracked bar in 3-point bending

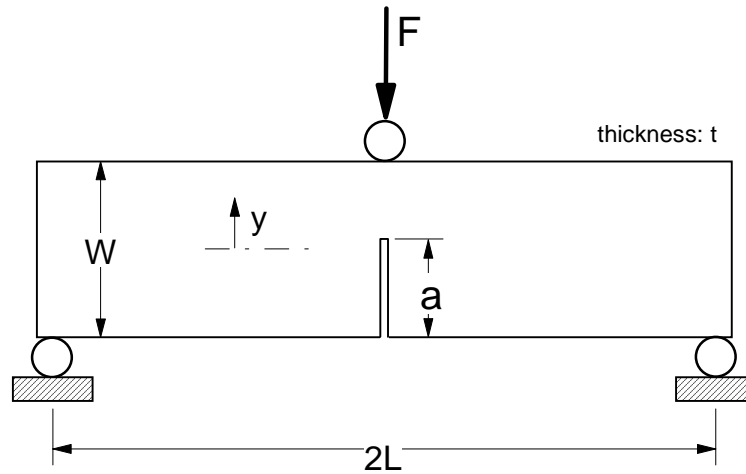


Fig. 10.6 3-point bending test.

Method: Green's function, using expansion with two regular terms, eqs.(10.4) and (10.5).
Stresses normal to the crack plane given by Filon [21]

$$\begin{aligned} \sigma_n = & -\frac{3yPL}{2tW^3} - \frac{4P}{tL} \sum_{n=1}^{\infty} \frac{\sinh(mW/2) - mW/2 \cosh(mW/2)}{mW + \sinh(mW)} \cos(mx) \cosh(my) \\ & - \frac{4P}{tL} \sum_0^{\infty} \frac{my \sinh(mW/2)}{mW + \sinh(mW)} \cos(mx) \sinh(my) \\ & - \frac{4P}{tL} \sum_{n=1}^{\infty} \frac{\cosh(MW/2) - MW/2 \sinh(MW/2)}{\sinh(MW) - MW} \cos(Mx) \sinh(My) \end{aligned}$$

$$-\frac{4P}{tL} \sum_0^{\infty} \frac{My \cosh(MW/2)}{\sinh(MW) - MW} \cos(Mx) \cosh(My) \quad (10.6)$$

$$m = \frac{2n\pi}{L}, \quad M = \frac{(2n+1)\pi}{L}$$

$$\sigma^* = \frac{3PL}{W^2 t}$$

$\alpha = a/W$	L/W=10	5	4	3	2.5	2
0	-0.526	-0.526	-0.526	-0.526	-0.526	-0.526
0.1	-0.29	-0.289	-0.287	-0.285	-0.283	-0.281
0.2	-0.146	-0.142	-0.140	-0.137	-0.134	-0.130
0.3	-0.038	-0.037	-0.037	-0.036	-0.035	-0.034
0.4	0.042	0.041	0.040	0.038	0.037	0.035
0.5	0.096	0.092	0.090	0.087	0.085	0.082
0.6	0.129	0.125	0.123	0.120	0.117	0.113
0.7	0.147	0.144	0.142	0.139	0.137	0.133
0.8	0.147	0.145	0.142	0.139	0.136	0.133
0.9	0.134	0.132	0.131	0.129	0.127	0.125
1	0.113	0.113	0.113	0.113	0.113	0.113

Table 10.5 T-stress $T/\sigma^*(1-a/W)^2$ for the edge-cracked bar in 3-point bending.

$\alpha = a/W$	L/W=5	4	3	2.5	2
0	-0.469	-0.469	-0.469	-0.469	-0.469
0.1	-0.332	-0.332	-0.331	-0.331	-0.330
0.2	-0.194	-0.191	-0.189	-0.187	-0.185
0.3	-0.058	-0.058	-0.058	-0.057	-0.056
0.4	0.072	0.071	0.068	0.067	0.064
0.5	0.178	0.175	0.171	0.168	0.164
0.6	0.262	0.259	0.255	0.250	0.244
0.7	0.325	0.322	0.317	0.314	0.307
0.8	0.35	0.344	0.338	0.332	0.326
0.9	0.337	0.334	0.332	0.330	0.327
1	0.302	0.302	0.302	0.302	0.302

Table 10.6 Biaxiality ratio in the form $\beta(1-a/W)^{1/2}$ for the edge-cracked bar in 3-point bending.

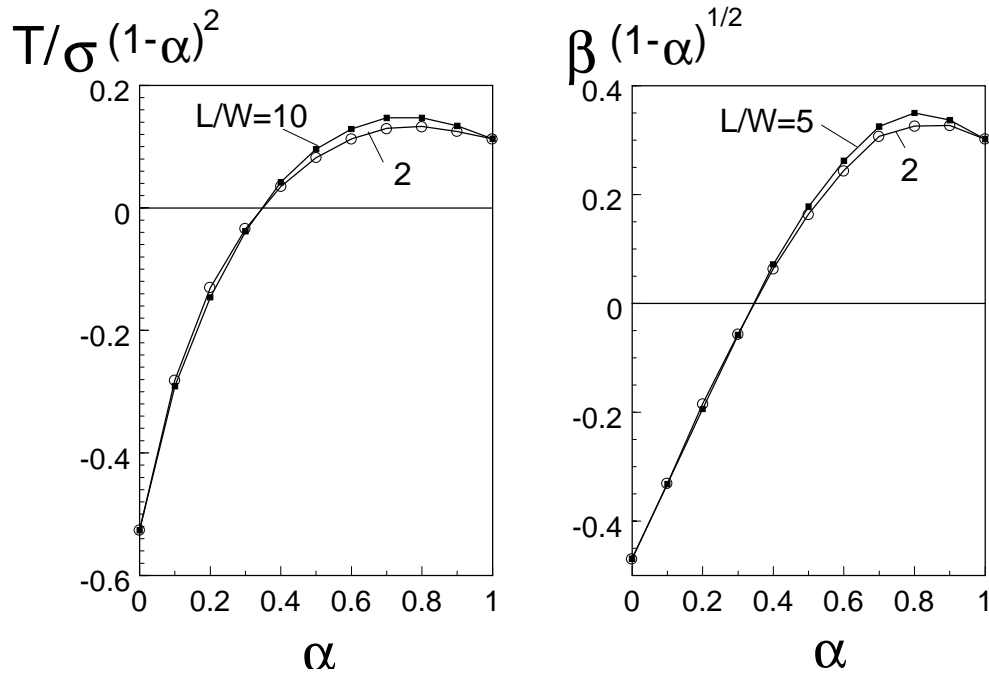


Fig. 10.7 T-stress and biaxiality ratio for 3-point bend tests.

10.4 The Double Cantilever Beam (DCB) specimen

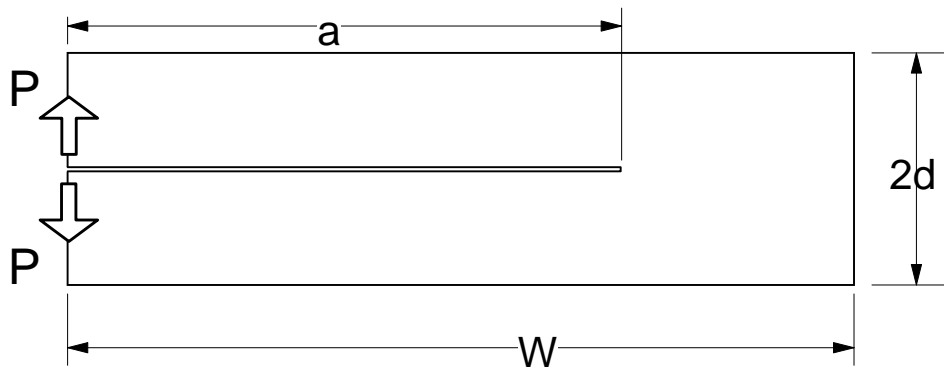


Fig. 10.8 Double-Cantilever-Beam specimen.

The biaxiality ratio β obtained for the DCB (Fig. 10.8) is found to be independent of a/W if $a/W < 0.55$. For $d/a < 0.5$ the biaxiality ratio can be described by the relation [11]

$$\frac{1}{\beta} \cong 0.681 \frac{d}{a} + 0.0685 \quad (10.7)$$

Using the stress intensity factor solution

$$K_I = \sqrt{\frac{12}{d}} P \left(\frac{a}{d} + 0.68 \right) \quad (10.8)$$

yields for the T-stress

$$T = \frac{\beta K_I}{\sqrt{\pi a}} \cong \sqrt{\frac{12}{\pi a d}} P \frac{a/d + 0.68}{0.681d/a + 0.0685} \quad (10.9)$$

10.5 Couple of opposite point forces

An infinitely long strip with a single edge crack is considered (Fig. 10.9). A pair of opposite point forces generates stresses in the plane of the crack.

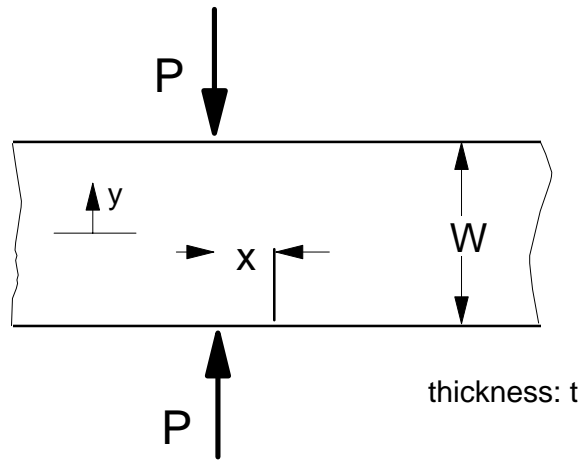


Fig. 10.9 Edge cracked strip with opposite concentrated forces.

Method: Green's function using expansion with two regular terms, eqs.(10.4) and (10.5).

The stresses normal to the plane of the crack, σ_n , are given by [21]

$$\begin{aligned} \sigma_n = & -\frac{4P}{\pi W t} \int_0^{\infty} \frac{\sinh u - u \cosh u}{\sinh 2u + 2u} \cos \frac{2ux}{W} \cosh \frac{2uy}{W} du - \\ & -\frac{4P}{\pi W t} \int_0^{\infty} \frac{2uy}{W} \frac{\sinh u}{\sinh 2u + 2u} \cos \frac{2ux}{W} \sinh \frac{2uy}{W} du \end{aligned} \quad (10.10)$$

$\alpha = a/W$	$x/W=0.1$	0.2	0.5	0.7	1.0	1.5
0.2	-0.355	0.273	0.143	0.054	0.009	0.00
0.3	-0.541	-0.027	0.209	0.119	0.034	0.001
0.4	-0.561	-0.169	0.226	0.159	0.053	0.002
0.5	-0.558	-0.213	0.226	0.171	0.060	0.003
0.6	-0.565	-0.180	0.225	0.160	0.053	0.002
0.7	-0.576	-0.046	0.219	0.127	0.037	0.001

Table 10.7 T-stress T/σ^* for the edge-cracked strip under opposite concentrated forces.

where

$$\sigma^* = \frac{P}{Wt} .$$

10.6 Rectangular plate with thermal stresses

A long rectangular plate with a parabolically distributed temperature Θ

$$\Theta = 4\Theta_0 \left[\frac{x}{W} - \left(\frac{x}{W} \right)^2 \right] \quad (10.11)$$

is considered, which causes a stress distribution

$$\sigma_y = \sigma^* \left(\frac{2}{3} - 4 \frac{x}{W} + 4 \frac{x^2}{W^2} \right), \quad \sigma^* = \alpha_T \Theta_0 E \quad (10.12)$$

with E = Young's modulus and α_T = thermal expansion coefficient. The stress distribution is shown in Fig. 10.10a. Introducing this stress distribution into eq.(10.5) and using the approximate Green's function (3.21), (3.23) yields the T-stress

$$\frac{T}{\sigma^*} = \frac{2}{3}(1-\alpha)^2 \left(1 + \frac{T_t}{\sigma_0} \right) + 4\alpha(1-\alpha) - \frac{2}{3} \quad (10.13)$$

where T_t is the reference T-stress solution for pure tension with tensile stress σ_0 taken from Table 10.1 or from eq.(10.1). The related stress intensity factor solution K , obtained with the weight function given in [9], has been entered additionally in Fig. 10.10b.

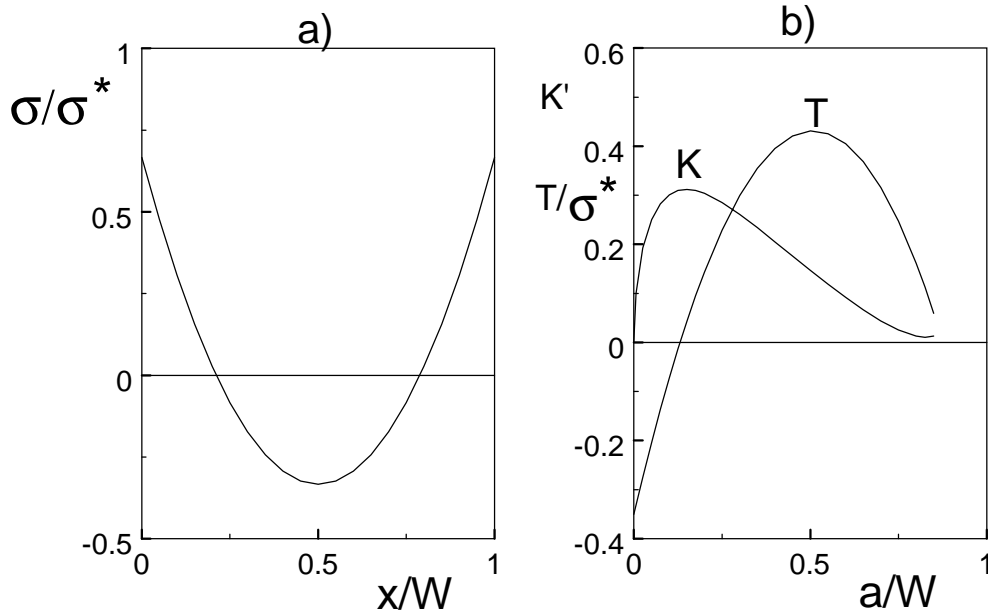


Fig. 10.10 a) thermal stresses in a rectangular plate, b) stress intensity factor and T-stress, $K' = K/(\sigma^* W^{1/2})$.

The biaxiality ratio represented in Fig. 10.11 was computed from the T-stress solution eq.(10.12) and the stress intensity factor solution K . Large positive biaxiality ratios are obvious for deep cracks. This is the consequence of the low stress intensity factors near $a/W = 0.8$.

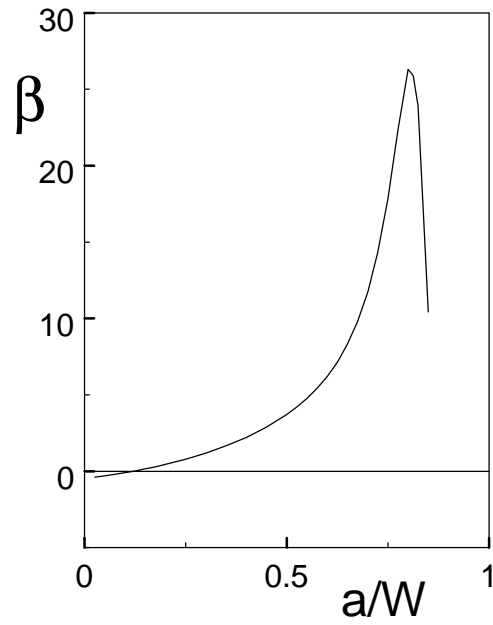


Fig. 10.11 Biaxiality ratio for thermal stress given by eq.(10.11).

10.7 Partially loaded rectangular plate

A plate loaded by a constant stress over a range d is shown in Fig. 10.12. The related T-stress terms T_d and the biaxiality ratios are entered into Tables 10.8-10.15.

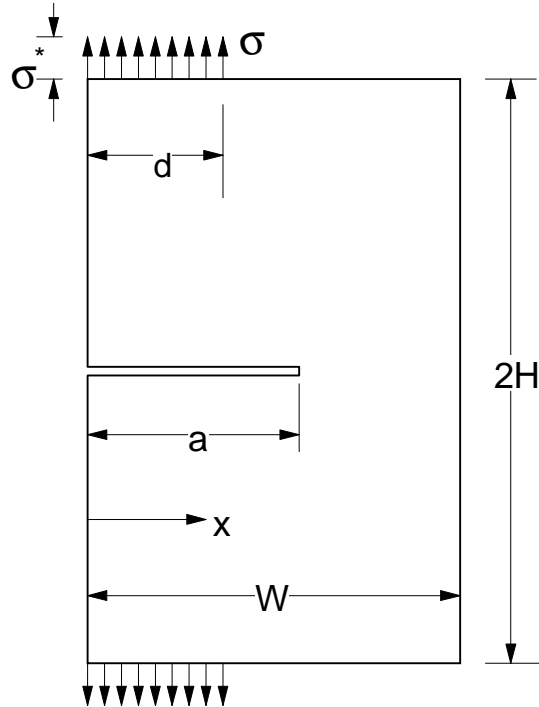


Fig. 10.12 Partially loaded edge-cracked rectangular plate.

$\alpha = a/W$	$d/W=0$	0.25	0.5	0.75	1.0
0.3	0	-0.196	-0.362	-0.501	-0.608
0.4	0	-0.072	-0.197	-0.372	-0.577
0.5	0	0.123	0.092	-0.102	-0.419
0.6	0	0.461	0.660	0.468	0.040
0.7	0	1.199	1.90	1.806	1.337

Table 10.8 T-stress T_d/σ^* for $H/W=1.25$.

$\alpha = a/W$	$d/W=0$	0.25	0.5	0.75	1.0
0.3	0	-0.174	-0.360	-0.515	-0.606
0.4	0	-0.042	-0.193	-0.383	-0.570
0.5	0	0.157	0.117	-0.409	-0.409
0.6	0	0.522	0.680	0.474	0.051
0.7	0	1.329	1.959	1.917	1.366

Table 10.9 T-stress T_d/σ^* for $H/W=1.00$.

$\alpha = a/W$	$d/W=0$	0.25	0.5	0.75	1.0
0.3	0	-0.094	-0.333	-0.524	-0.571
0.4	0	0.098	-0.115	-0.369	-0.485
0.5	0	0.348	0.251	-0.039	-0.277
0.6	0	0.703	0.808	0.560	0.199
0.7	0	1.456	2.052	2.011	1.485

Table 10.10 T-stress T_d/σ^* for $H/W=0.75$.

$\alpha = a/W$	$d/W=0$	0.25	0.5	0.75	1.0
0.3	0	0.257	-0.119	-0.317	-0.299
0.4	0	0.722	0.457	0.136	0.110
0.5	0	1.157	1.195	0.783	0.666
0.6	0	1.614	2.007	1.668	1.372
0.7	0	2.250	3.174	3.007	2.593

Table 10.11 T-stress T_d/σ^* for $H/W=0.50$.

$\alpha = a/W$	$d/W=0.25$	0.5	0.75	1.0
0.3	-0.156	-0.184	-0.225	-0.311
0.4	-0.045	-0.077	-0.124	-0.213
0.5	0.056	0.026	-0.024	-0.105
0.6	0.142	0.122	0.073	0.006
0.7	0.209	0.213	0.160	0.116

Table 10.12 Biaxiality ratio $\beta(1-a/W)^{1/2}$ for $H/W=1.25$.

$\alpha = a/W$	$d/W=0.25$	0.5	0.75	1.0
0.3	-0.138	-0.181	-0.230	-0.306
0.4	-0.026	-0.074	-0.129	-0.209
0.5	0.071	0.032	0.026	-0.102
0.6	0.154	0.124	0.073	0.008
0.7	0.227	0.205	0.167	0.118

Table 10.13 Biaxiality ratio $\beta(1-a/W)^{1/2}$ for $H/W=1.00$.

$\alpha = a/W$	$d/W=0.25$	0.5	0.75	1.0
0.3	-0.071	-0.164	-0.235	-0.284
0.4	0.059	-0.044	-0.125	-0.176
0.5	0.153	0.068	-0.009	-0.069
0.6	0.209	0.149	0.086	0.031
0.7	0.251	0.216	0.175	0.128

Table 10.14 Biaxiality ratio $\beta(1-a/W)^{1/2}$ for $H/W=0.75$.

$\alpha = a/W$	$d/W=0.25$	0.5	0.75	1.0
0.3	0.166	-0.054	-0.135	-0.136
0.4	0.378	0.158	0.043	0.037
0.5	0.488	0.329	0.177	0.157
0.6	0.466	0.355	0.248	0.209
0.7	0.386	0.332	0.261	0.222

Table 10.15 Biaxiality ratio $\beta(1-a/W)^{1/2}$ for $H/W=0.50$.

An example of application of this loading case may be demonstrated for a plate with $H/W = 1.25$ loaded by a couple of point forces P at several locations d/W as illustrated in Fig. 10.13a. The evaluation of the related T-stress term is explained in Fig. 10.13b.

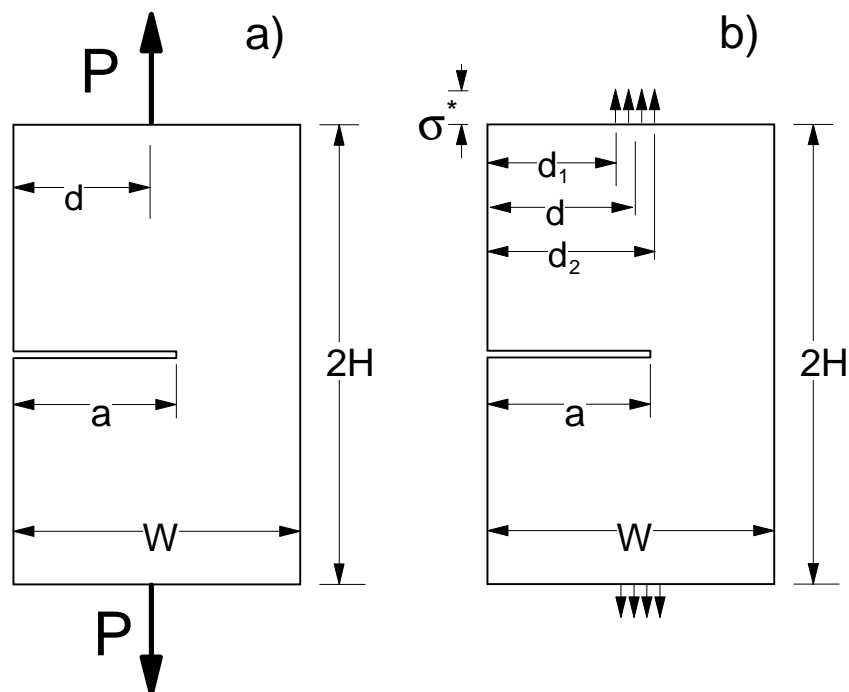


Fig. 10.13 Computation of T-stresses in plates loaded by a couple of point forces.

First, we determine the T_d/σ^* -values for two values d_1 and d_2 with $d_1 = d - \varepsilon$ and $d_2 = d + \varepsilon$ ($\varepsilon \ll d$) by interpolation of the tabulated results applying cubic splines. The normal force P is given by

$$P = \sigma^* (d_2 - d_1)t \quad (10.14)$$

(t = thickness). The T-stress for this case is

$$T_P = \left(\frac{T_{d_2}}{\sigma^*} - \frac{T_{d_1}}{\sigma^*} \right) \sigma^* = \left(\frac{T_{d_2}}{\sigma^*} - \frac{T_{d_1}}{\sigma^*} \right) \frac{P}{t(d_2 - d_1)} \quad (10.15)$$

and for the case of $d_1, d_2 \rightarrow d$ ($\varepsilon \rightarrow 0$)

$$T_P = \frac{\partial(T_d / \sigma^*)}{\partial(d / W)} \frac{P}{Wt} \quad (10.16)$$

In Fig. 10.14 the T-stresses are plotted as a function of the relative crack length a/W .

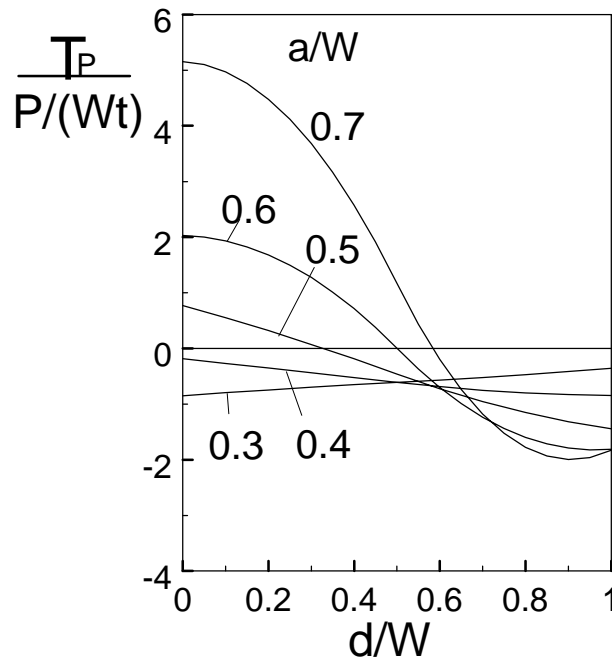


Fig. 10.14 T-stress caused by a couple of forces acting at location d ($H/W = 1.25$).

These results can be used to compute the T-stress for any given distribution of normal tractions σ_n at the ends of the plate

$$T = \frac{1}{W} \int_0^W \frac{T_P}{\sigma^*} \sigma_n(x) dx \quad , \quad \sigma^* = \frac{P}{Wt} \quad (10.17)$$

If a smooth distribution of normal tractions acts at the ends of the plate it is of advantage to rewrite eq.(10.17) and to apply integration by parts. This leads to

$$T = \frac{T_d}{\sigma^*} \sigma_n \Big|_{x=d=W} - \int_0^W \frac{T_d}{\sigma^*} \frac{d\sigma}{dx} dx. \quad (10.18)$$

As an example the T-stress for bending was computed from (10.18). The results for two values of H/W are shown in Fig. 10.15 (circles) together with the data of Table 10.2 (curves) which were obtained directly from BCM-computations. The agreement is good.

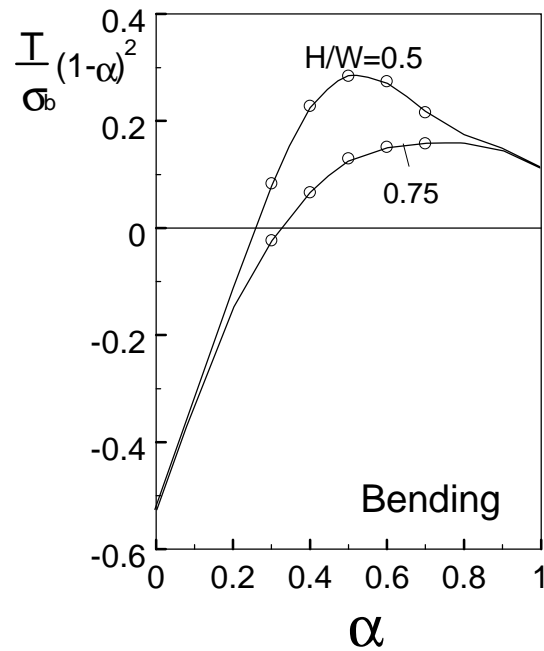


Fig. 10.15 Comparison of bending results obtained with eq.(10.18) (circles) and with BCM (curves).

11 Edge-cracked circular disk

Edge-cracked circular disks are often used as fracture mechanics test specimens, especially in case of ceramic materials [22][23]. Figure 11.1 shows the geometric data.

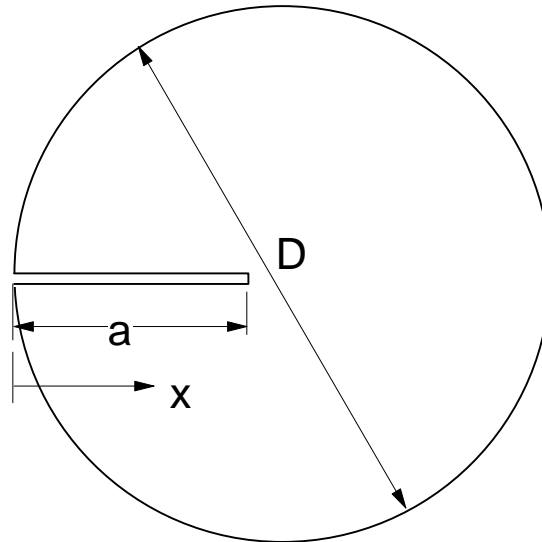


Fig. 11.1 Geometric data of an edge-cracked circular disk.

11.1 Circumferentially loaded disk

A circular disk is loaded by constant normal tractions σ_n along the circumference (loading as in Fig.7.1)

$$\sigma_n = \text{const} , \quad \tau = 0 \quad (11.1)$$

In this case it holds [9]

$$A^*_0 (1 - \alpha)^2 = -0.11851 = C^*_0 , \quad \alpha = a / W \quad (11.2)$$

and, from eq.(2.7)

$$\frac{T}{\sigma_n} = -(4A^*_0 + 1) = \frac{0.474}{(1 - \alpha)^2} - 1 \quad (11.3)$$

The value C^*_0 , occurring in eq.(11.2) is identical with the coefficient of Wigglesworth's [24] expansion for the edge-cracked semi-infinite body.

With the stress intensity factor solution

$$K_I = \sigma_n F \sqrt{\pi a} , \quad F = \frac{1.1215}{(1-\alpha)^{3/2}} \quad (11.4)$$

the biaxiality ratio results as

$$\beta = \frac{0.4227}{\sqrt{1-\alpha}} - 0.8917(1-\alpha)^{3/2} \quad (11.5)$$

11.2 Diametrically loaded disk

11.2.1 Load perpendicular to the crack

The Green's function method may be applied here to the diametrically loaded edge-cracked disk (Fig. 11.2).

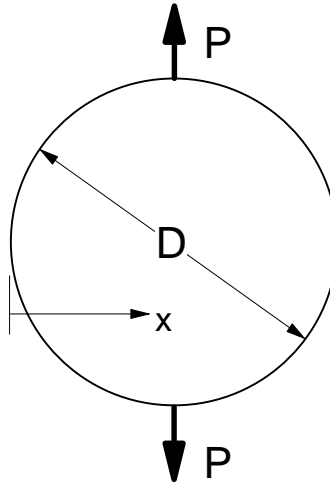


Fig. 11.2 Diametrically loaded circular disk.

Using eq.(11.3) as the reference T-stress solution the coefficient C for the Green's function, represented by eqs.(3.22) and (3.23), follows as

$$C = \frac{0.9481}{a(1-\alpha)^2}, \quad \alpha = a / D \quad (11.6)$$

Consequently, the T-stress can be computed from

$$T = \frac{0.9481}{(1-\alpha)^2} \int_0^1 (1-\rho) \sigma_y(\rho) d\rho - \sigma_y \Big|_{x=a}, \quad \rho = x / a \quad (11.7)$$

As an application a disk of unit thickness is considered, which is diametrically loaded by a pair of forces P . The forces may act perpendicular to the crack plane. In this case the stresses are given by

$$\frac{\sigma_y}{\sigma^*} = \frac{4}{[1+(1-\xi)^2]^2} - 1, \quad \xi = x/R, R = D/2 \quad (11.8)$$

$$\frac{\sigma_x}{\sigma^*} = 1 - \frac{4(1-\xi)^2}{[1+(1-\xi)^2]^2}, \quad \sigma^* = \frac{P}{\pi R} \quad (11.9)$$

as illustrated in Fig. 11.3. Introducing σ_y in eq.(3.22) yields the T-stress term

$$T \cong \frac{0.9481\sigma^*}{(1-\alpha)^2(a/R)^2} \left[4\left(1 - \frac{a}{R}\right) \arctan\left(1 - \frac{a}{R}\right) + 2\frac{a}{R} - \frac{a^2}{R^2} - \pi\left(1 - \frac{a}{R}\right) \right] - \sigma_y \Big|_{x=a} \quad (11.10)$$

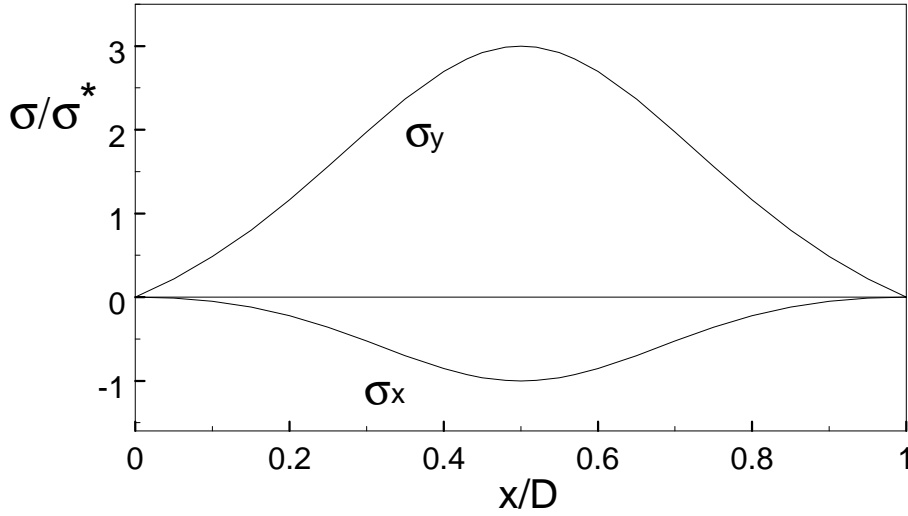


Fig. 11.3 Stresses along the x-axis in a diametrically loaded disk.

The stress intensity factor results from [15] as

$$K_I = \int_0^a h(x,a) \sigma_y dx \quad (11.11)$$

where h is the fracture mechanics weight function. In case of an edge-cracked disk a representation is given in [9], i.e.

$$h(x,a) = \sqrt{\frac{2}{\pi a}} \left[\frac{\rho}{\sqrt{1-\rho}} + D_0 \sqrt{1-\rho} + D_1 (1-\rho)^{3/2} + D_2 (1-\rho)^{5/2} \right] \quad (11.12)$$

with the coefficients

$$\begin{aligned} D_0 &= (1.5721 + 2.4109\alpha - 0.8968\alpha^2 - 1.4311\alpha^3) / (1-\alpha)^{3/2} \\ D_1 &= (0.4612 + 0.5972\alpha + 0.7466\alpha^2 + 2.2131\alpha^3) / (1-\alpha)^{3/2} \\ D_2 &= (-0.2537 + 0.4353\alpha - 0.2851\alpha^2 - 0.5853\alpha^3) / (1-\alpha)^{3/2} \end{aligned} \quad (11.13)$$

By consideration of the total x-stress (crack contribution and x-stress component in the uncracked body), one can define the additional biaxiality ratio

$$\tilde{\beta} = T' \frac{\sqrt{\pi a}}{K_I} \quad (11.14)$$

The T-stress and the stress intensity factor result in the biaxiality ratios $\beta, \tilde{\beta}$ which are shown as curves in Fig. 11.4.

In addition to the Green's function computations, the biaxiality ratios were directly determined with the Boundary Collocation method (BCM) which provides the coefficient A^*_0 and by eq.(2.8) the quantity T' for the situation of diametrical loading. The results - expressed by $\tilde{\beta}$ - are entered as circles. An excellent agreement is obvious between The BCM results and those obtained from the Green's function representation. This is an indication of an adequate description of the Green's function by the set-up eq.(3.22) using only one regular term.

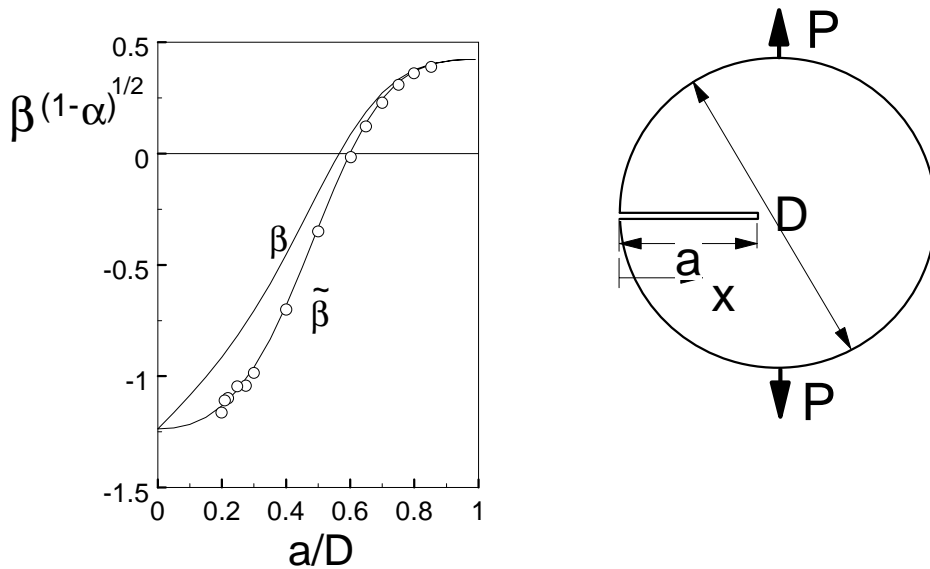


Fig. 11.4 Biaxiality ratio for an edge-cracked circular disk diametrically loaded by a pair of forces; lines: eq.(11.10), circles: BCM-results.

11.2.2 Brazilian disk (edge-cracked)

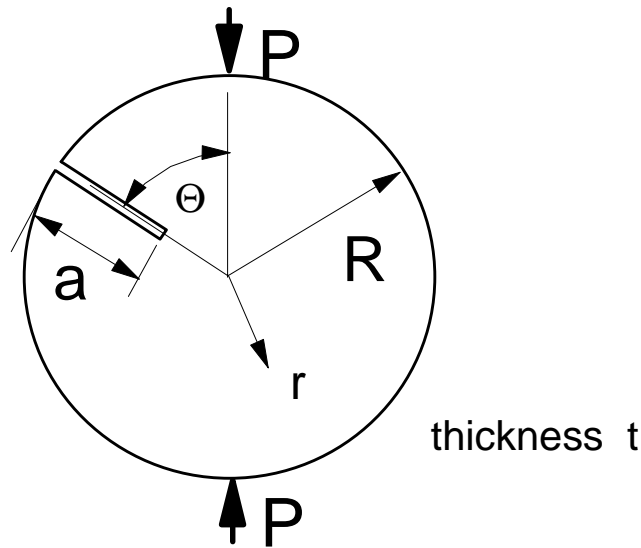


Fig. 11.5 Brazilian disk test with edge-cracked disk.

The circumferential stress component in an uncracked Brazilian disk has been given by Erdlac (quoted in [25]) as

$$\sigma_{\varphi} = \sigma_n = \frac{2P}{\pi R} \left[\frac{1}{2} - \frac{(1 - \rho \cos \Theta) \sin^2 \Theta}{(1 + \rho^2 - 2\rho \cos \Theta)^2} - \frac{(1 + \rho \cos \Theta) \sin^2 \Theta}{(1 + \rho^2 + 2\rho \cos \Theta)^2} \right], \quad \rho = r / R \quad (11.15)$$

Using eq.(11.7) the T-stress can be determined. The T-stress term, evaluated for several relative crack depths a/W and several angles Θ is compiled in Table 11.1, the biaxiality ratio in Table 11.2.

$\alpha = a/2R$	$\Theta = \pi/16$	$\pi/8$	$\pi/4$	$3\pi/8$	$7\pi/16$	$\pi/2$
0	0	0	0	0	0	0
0.05	2.671	1.086	0.359	0.215	0.191	0.184
0.1	0.933	1.466	0.715	0.460	0.415	0.401
0.2	-1.687	0.194	1.068	0.979	0.937	0.922
0.3	-2.319	-1.099	0.691	1.328	1.428	1.456
0.4	-2.546	-1.824	-0.078	1.235	1.577	1.691
0.5	-2.744	-2.310	-0.896	0.518	0.952	1.104
0.6	-3.050	-2.814	-1.906	-1.153	-0.959	-0.894
0.65	-3.290	-3.163	-2.727	-2.637	-2.662	-2.675
0.7	-3.637	-3.683	-4.085	-4.911	-5.196	-5.297

Table 11.1 T-stress T/σ^* for the Brazilian disk test ($\sigma^* = 2P/(\pi R)$).

For the determination of the total x-stress at the crack tip (i.e. the determination of T') the radial stress component has to be included, which was also derived by Erdlac

$$\sigma_r = \frac{2P}{\pi R} \left[\frac{1}{2} - \frac{(1 - \rho \cos \Theta)(\cos \Theta - \rho)^2}{(1 + \rho^2 - 2\rho \cos \Theta)^2} - \frac{(1 + \rho \cos \Theta)(\cos \Theta + \rho)^2}{(1 + \rho^2 + 2\rho \cos \Theta)^2} \right] \quad (11.16)$$

$\alpha = a/2R$	$\Theta = \pi/16$	$\pi/8$	$\pi/4$	$3\pi/8$	$7\pi/16$	$\pi/2$
0	-1.229	-1.23	-1.22	-1.23	-1.23	-1.230
0.05	-0.874	-1.081	-1.143	-1.154	-1.155	-1.155
0.1	-0.259	-0.793	-1.023	-1.069	-1.077	-1.080
0.2	0.614	-0.079	-0.681	-0.865	-0.899	-0.910
0.3	1.011	0.441	-0.286	-0.611	-0.681	-0.702
0.4	1.155	0.686	0.023	-0.338	-0.424	-0.452
0.5	1.149	0.726	0.189	-0.088	-0.153	-0.174
0.6	1.037	0.641	0.256	0.118	0.092	0.084
0.65	0.948	0.574	0.277	0.205	0.192	0.188
0.7	0.841	0.502	0.302	0.274	0.272	0.272
1	0.423	0.423	0.423	0.423	0.423	0.423

Table 11.2 Biaxiality ratio $\beta(1-a/D)^{1/2}$ for the Brazilian disk test.

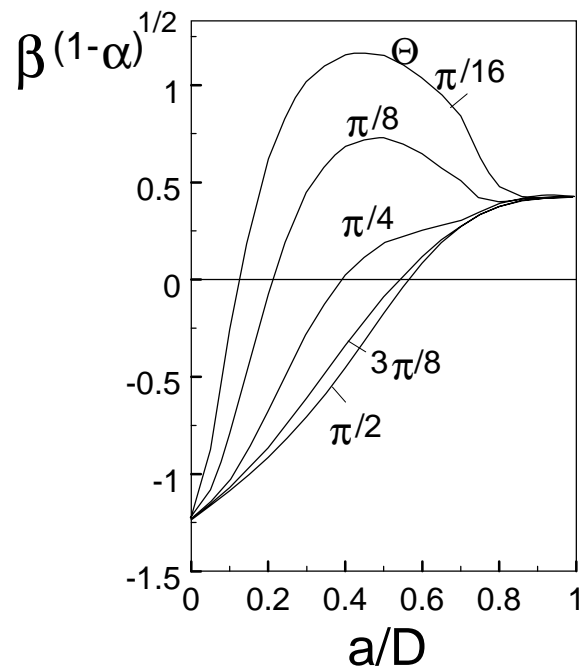


Fig.11.6 Biaxiality ratio $\beta(1-\alpha)^{1/2}$ for the Brazilian disk test, $\alpha = a/D$.

11.2.3 Disk with thermal stresses

In a thermally loaded circular disk the stresses in the absence of a crack consist of the circumferential stress component σ_ϕ and of the radial stress distribution σ_r . The two stress components can be computed from the temperature distribution $\Theta(r)$ with $r = D/2 - x$ (see e.g. [26])

$$\sigma_r = \alpha_T E \left(\frac{1}{R^2} \int_0^R \Theta r dr - \frac{1}{r^2} \int_0^r \Theta r dr \right) \quad (11.17)$$

$$\sigma_\phi = \alpha_T E \left(\frac{1}{R^2} \int_0^R \Theta r dr + \frac{1}{r^2} \int_0^r \Theta r dr - \Theta \right) \quad (11.18)$$

with the thermal expansion coefficient α_T . The temperatures found e.g. in [23] can be expressed by

$$\Theta(r) = \Theta_0 \left[1 + B_2 \left(\frac{r}{R} \right)^2 + B_4 \left(\frac{r}{R} \right)^4 \right] \quad (11.19)$$

with the maximum temperature occurring in the centre of the disk ($r = 0$). The related stresses are given by

$$\sigma_\phi = \alpha_T E \Theta_0 \left[\frac{1}{4} B_2 + \frac{1}{6} B_4 - \frac{3}{4} B_2 \left(\frac{r}{R} \right)^2 - \frac{5}{6} B_4 \left(\frac{r}{R} \right)^4 \right] \quad (11.20)$$

$$\sigma_r = \alpha_T E \Theta_0 \left[\frac{1}{4} B_2 \left(1 - \frac{r^2}{R^2} \right) + \frac{1}{6} B_4 \left(1 - \frac{r^4}{R^4} \right) \right] \quad (11.21)$$

For a typical stress distribution in a thermally heated disk one can conclude from curves plotted in [23]

$$\sigma_\phi = -\sigma^* \left[1 - \frac{9}{2} \left(\frac{r}{R} \right)^2 + \frac{5}{2} \left(\frac{r}{R} \right)^4 \right] \quad (11.22)$$

$$\sigma_r = -\sigma^* \left[1 - \frac{3}{2} \left(\frac{r}{R} \right)^2 + \frac{1}{2} \left(\frac{r}{R} \right)^4 \right] \quad (11.23)$$

where σ^* is the circumferential tensile stress at $r = R$. The stresses are and shown in Fig. 11.7.

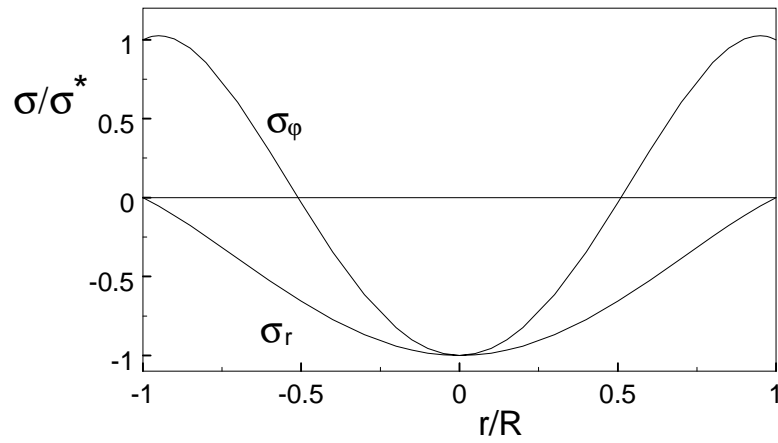


Fig. 11.7 Stress distributions in a thermally heated disk.

When eq.(11.7) is used, the thermal stresses result in the T-stress

$$T \cong -0.15801 \sigma^* \left[2 \left(\frac{a}{R} \right)^2 - 4 \frac{a}{R} - 3 \right] - \sigma_y \Big|_{x=a} \quad (11.24)$$

Including the σ_x -stress, present already in the uncracked disk, it results with eq.(2.8)

$$\frac{T'}{\sigma^*} = \frac{T}{\sigma^*} + \frac{\sigma_r}{\sigma^*} \Big|_{x=a} \quad (11.25)$$

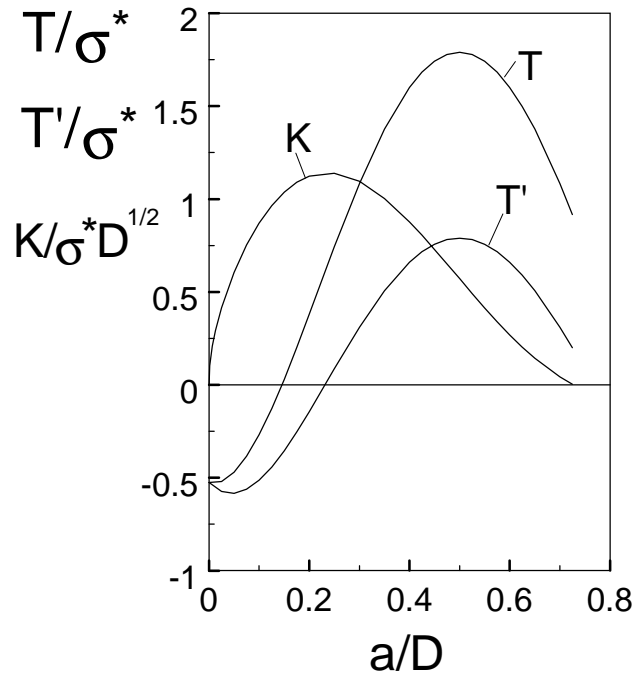


Fig. 11.8 Stress intensity factor and T-stress for a disk under thermal loading.

The two T-stresses are plotted in Fig. 11.8 together with the stress intensity factor computed with the weight function for the edge-cracked disk.

The biaxiality ratio β and the effective biaxiality ratio $\tilde{\beta}$, defined by eq.(11.14), are plotted in Fig. 11.9. Very high β -values occur for $a/D > 0.6$. The main reason is the very small stress intensity factor which disappears at approximately $a/D = 0.7$.

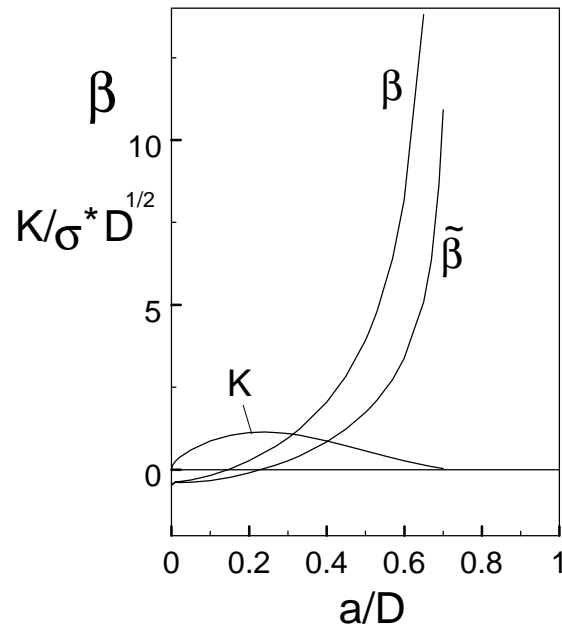


Fig. 11.9 Stress intensity factor K , biaxiality ratio β , and effective biaxiality ratio $\tilde{\beta}$, defined by eq.(11.14).

12 Cracks ahead of notches

Special specimens contain narrow notches which are introduced in order to simulate a starter crack. This is for instance the case in fracture toughness experiments carried out on ceramics. A plate with a slender edge notch of depth a_0 is considered. A small crack of length ℓ is assumed to occur directly at the notch root with the radius R . The geometrical data are illustrated in Fig. 12.1.

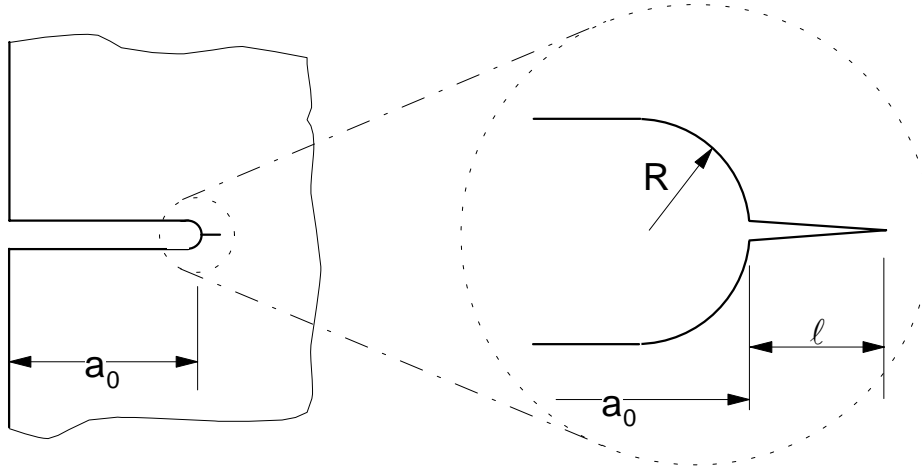


Fig. 12.1 A small crack emanating from the root of a notch.

In the absence of a crack the stresses near the notch root are given by

$$\sigma_y = \frac{2K(a_0)}{\sqrt{\pi(R+2\xi)}} \frac{R+\xi}{R+2\xi}$$

$$\sigma_x = \frac{2K(a_0)}{\sqrt{\pi(R+2\xi)}} \frac{\xi}{R+2\xi}$$
(12.1)

(for ξ see Fig. 12.1) as shown by Creager and Paris [26]. The quantity $K(a_0)$ is the stress intensity factor of a crack with same length a_0 as the notch under identical external load

$$K(a_0) = \sigma^* F(a_0) \sqrt{\pi a_0}$$
(12.2)

with the characteristic stress σ^* and the geometric function F . The stresses resulting from eq.(12.1) are plotted in Fig. 12.2. The solid parts of the curves represent the region ($0 \leq \xi \leq R/2$) where higher order terms are negligible. A small crack of length ℓ is considered which emanates from the notch root (Fig. 12.1).

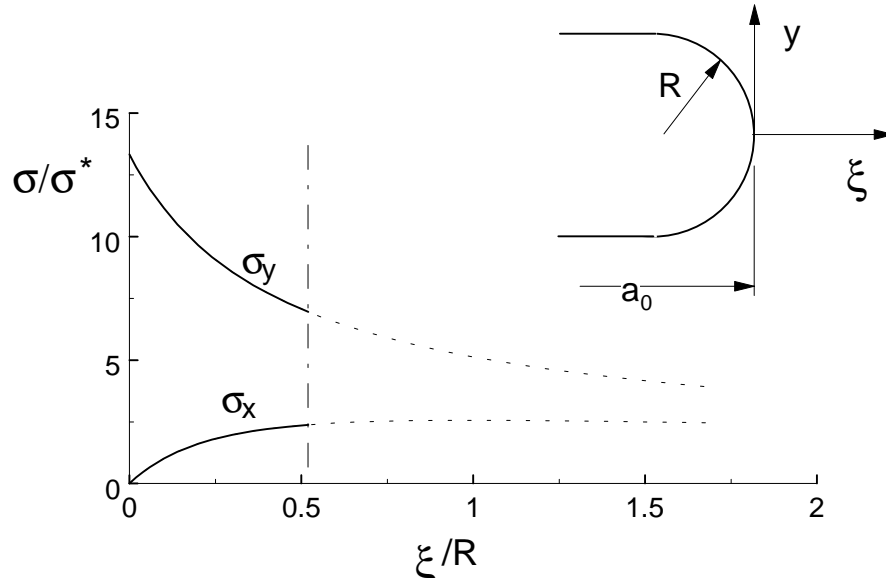


Fig. 12.2 Stresses ahead of a slender notch computed according to Creager and Paris [26] for $a_0/W = 0.5$ and $R/W = 0.025$.

Under externally applied load the coefficients of the stress function were calculated with BCM applying the outer fiber bending stress as the reference stress, i.e.

$$\sigma^* = \sigma_b = \frac{6M}{W^2 t} \quad (12.4)$$

with specimen width W , thickness t and bending moment M . The coefficient A_0 is related to the stress intensity factor K_I by

$$K_I = \sigma^* F(\ell) \sqrt{\pi \ell}, \quad F(\ell) = \sqrt{18W / \ell} A_0 \quad (12.5)$$

with the geometric function F . The T-term T' , eq.(2.8), results directly from the coefficient A_0 . In Fig. 12.3 the term T' is plotted versus a/W the relative for several notch depths a_0 . Additionally, the "long crack solution" given by eq.(10.2) is introduced as solid curve. This curve represents the T-stress for an edge crack of total length $a = a_0 + \ell$.

Results obtained under tensile loading are plotted in Fig. 12.4. In this case the characteristic stress is identical with the remote tensile stress σ_0 , i.e. $\sigma^* = \sigma_0$. In this representation the solid line is described by eq.(10.1).

For the limit case $\ell/R \rightarrow 0$ the T-stress can be determined from the solution for a small crack in a semi-infinite plate with a tensile stress identical with the maximum normal stress σ_{\max} occurring directly at the notch root

$$\sigma_{\max} = 2\sigma^* F(a_0) \sqrt{\frac{a_0}{R}} \quad (12.6)$$

Directly at the free surface ($\xi = 0$) it holds $\sigma_x = 0$ and, therefore, $T' = T$ for $\ell/R \rightarrow 0$. It can be concluded

$$T_0 = T_{\ell/R \rightarrow 0} = \left. \frac{T_{plate}}{\sigma^*} \right|_{\alpha \rightarrow 0} \sigma_{max} \quad (12.7)$$

$$\left. \frac{T_{plate}}{\sigma^*} \right|_{\alpha \rightarrow 0} = -4(A^*_0)_{plate, \alpha \rightarrow 0} = -0.526 \quad (12.8)$$

and, consequently,

$$\frac{T_0}{\sigma^*} = -1.052 F(a_0) \sqrt{\frac{a_0}{R}} \quad (12.9)$$

It becomes obvious from eq.(12.9) that for slender notches very strong compressive T-stresses occur in the limit case $\ell/R \rightarrow 0$. The limit values T_0 for tension and bending, indicated by the arrows in Figs. 12.3 and 12.4, are entered in Table 12.1.

In Fig. 12.5 both the bending and the tensile results are plotted in a normalised representation. From Fig. 12.5b we can conclude that the deviation between the T-stress term for the crack/notch configuration and the long-crack solution T^* (with the crack assumed to have the total length $a_0 + \ell$) is negligible for $\ell/R > 1$. The drastic decrease in T for $\ell/R \rightarrow 0$ must occur within the range $0 < \ell/R < 0.2$.

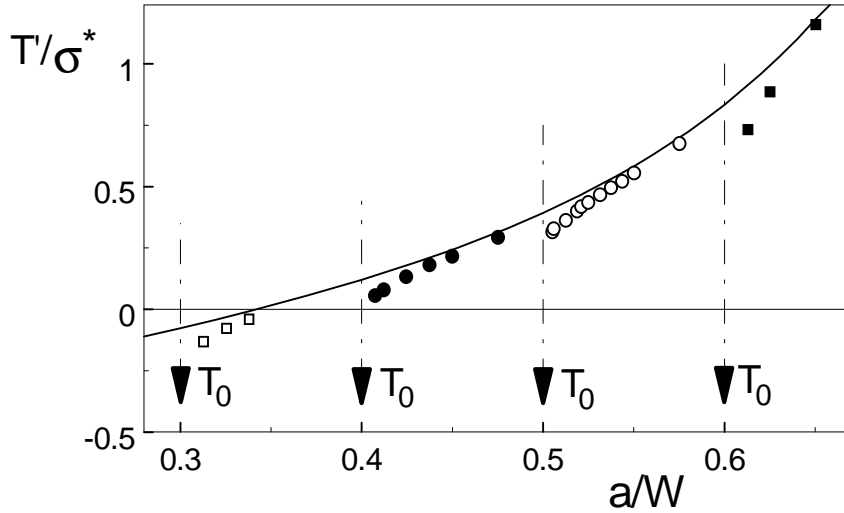


Fig. 12.3 T-stress for a small crack ahead of a slender notch in bending, computed with the Boundary Collocation Method for $R/W = 0.025$. Solid line: long-crack solution.

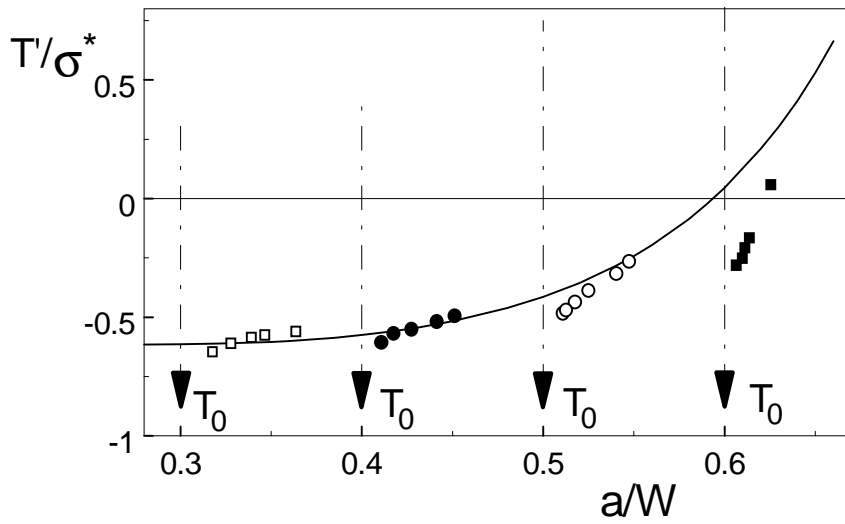


Fig. 12.4 T-stress for a small crack ahead of a slender notch in tension, computed with the Boundary Collocation Method for $R/W = 0.025$. Solid line: long-crack solution.

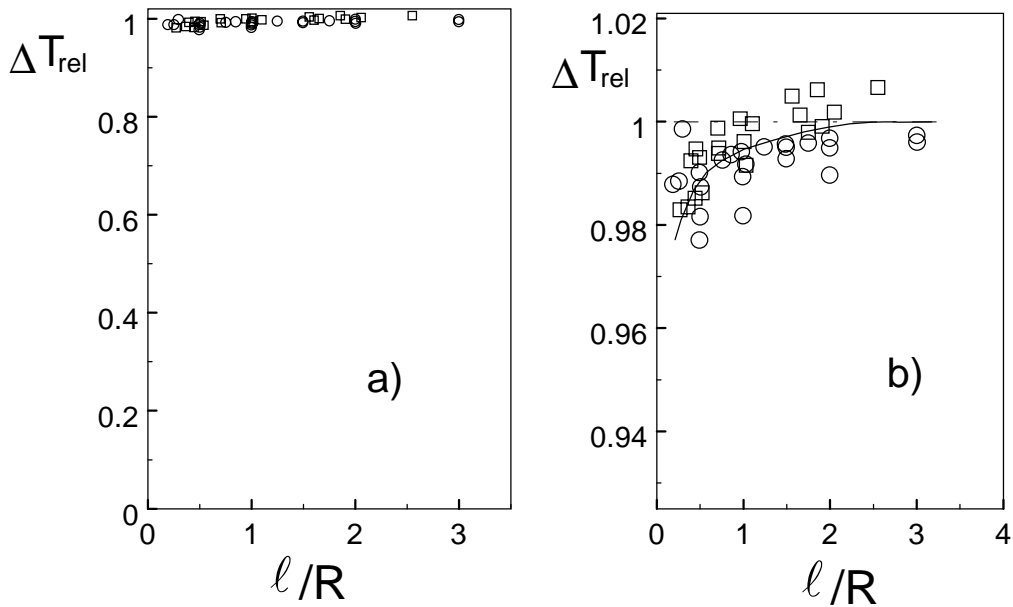


Fig. 12.5 T-stress in a normalised representation $\Delta T_{rel} = (T' - T_0)/(T^* - T_0)$, T^* =long-crack solution; circles: tension, squares: bending.

a/W	T_0/σ^* (bending)	T_0/σ^* (tension)
0.3	-4.11	-6.05
0.4	-5.28	-8.91
0.5	-7.01	-13.31
0.6	-9.86	-20.74

Table 12.1 Limit values for the T-stress term ($l/R \rightarrow 0$).

13 Array of deep edge cracks

Figure 13.1 shows an array of periodical edge cracks. BCM-computations were performed for an element of periodicity for the special case of a constant remote tensile stress σ . The boundary conditions are given by constant displacements v and disappearing shear stresses along the symmetry lines, i.e.

$$v = \frac{\sigma d}{E'} \frac{1}{2}; \quad \tau_{xy} = 0 \quad \text{for } y = \pm d/2 \quad (13.1)$$

($E' = E$ for plane stress and $E' = E/(1-\nu^2)$ for plane strain, $E =$ Young's modulus, $\nu =$ Poisson's ratio) as illustrated in Fig. 13.2. The coefficient A^*_0 is shown in Fig. 13.3a as a function of the ratio d/a for different relative crack lengths $\alpha = a/W$. The result can be summarised as

$$A^*_0 = 0.148, \quad d/a \leq 1.5 \quad (13.2)$$

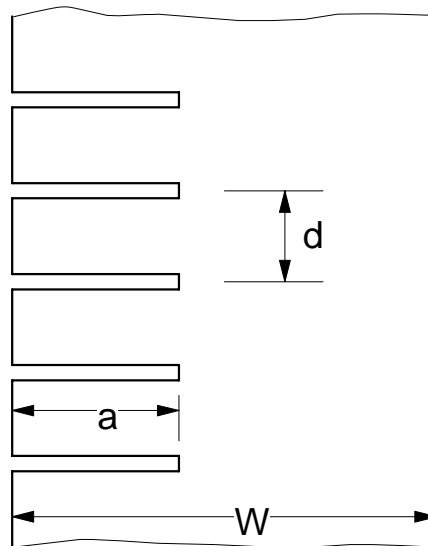


Fig. 13.1 Periodical edge cracks in an endless strip.

The coefficient A_0 is plotted in Fig. 13.3b in the normalised form

$$\tilde{A}_0 = 6A_0 \sqrt{\pi W / d} \quad (13.3)$$

For all values $\alpha = a/W$ investigated it was found

$$\tilde{A}_0 = 1.000 \pm 0.002 \quad (13.4)$$

resulting in the stress intensity factor solution

$$K_I = \sigma \sqrt{d/2} \quad (13.5)$$

(see e.g. [27]). The T-stress term T' is

$$T' = -0.592 \sigma \quad (13.6)$$

and the biaxiality ratio $\tilde{\beta}$ according to eq.(11.14) results as

$$\tilde{\beta} = -1.484 \sqrt{a/d} \quad (13.7)$$

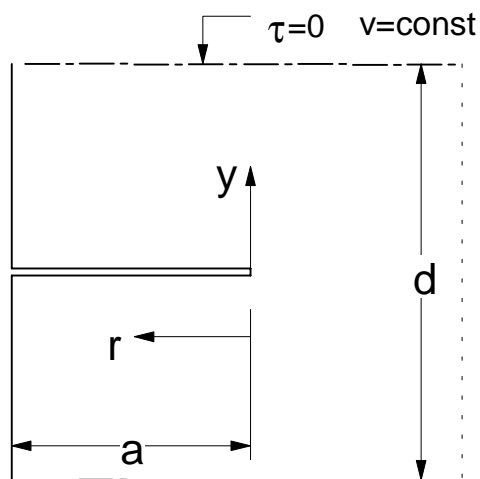


Fig. 13.2 Boundary conditions representing an endless strip with periodical cracks.

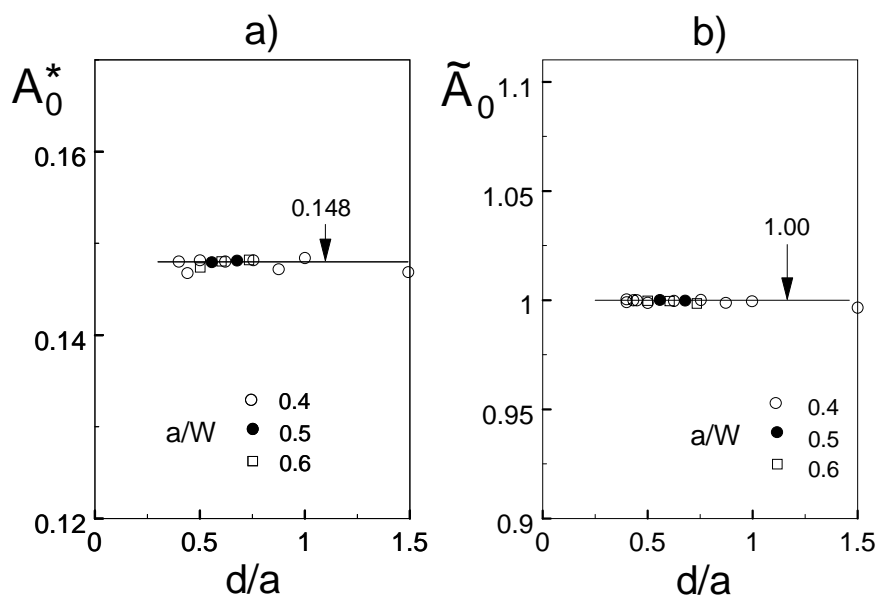


Fig. 13.3 a) Influence of the geometric data on the first regular term of the Williams stress function A_0^* , b) Coefficient A_0 in the normalisation $\tilde{A} = 6A_0 \sqrt{\pi W/d}$.

14 Double-edge-cracked plate

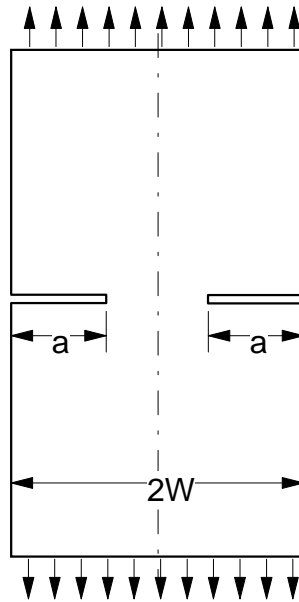


Fig. 14.1 Double-edge-cracked rectangular plate

$\alpha = a/W$	$H/W=1.5$	1.25	1.00	0.75	0.50	0.35
0.0	-0.526	-0.526	-0.526	-0.526	-0.526	-0.526
0.1	-0.530	-0.530	-0.530			
0.2	-0.532	-0.528	-0.527			
0.3	-0.532	-0.520	-0.512	-0.473	-0.257	0.293
0.4	-0.528	-0.503	-0.440	-0.282	0.256	1.546
0.5	-0.522	-0.464	-0.316	0.045	1.058	3.135
0.6	-0.510	-0.409	-0.153	0.483	2.202	5.24
0.7	-0.49	-0.32	0.023	0.969	3.68	8.13

Table 14.1 T-stress T/σ^* for the Double-edge-cracked plate in tension.

For the long plate ($H/W \geq 1.5$) the relations hold within $0 \leq \alpha \leq 0.7$

$$T / \sigma = -0.526 - 0.0438 \alpha + 0.0444 \alpha^2 + 0.12194 \alpha^3 \quad (14.1)$$

$$\beta = -0.469 - 0.07104 \alpha + 0.1196 \alpha^2 + 0.2801 \alpha^3 \quad (14.2)$$

and for the quadratic plate ($H/W=1$)

$$T / \sigma = -0.526 + 0.1804 \alpha - 2.7241 \alpha^2 + 9.5966 \alpha^3 - 6.3883 \alpha^4 \quad (14.3)$$

$$\beta = -0.469 + 0.1229 \alpha - 1.2256 \alpha^2 + 6.0628 \alpha^3 - 4.4983 \alpha^4 \quad (14.4)$$

$\alpha=a/W$	H/W=1.5	1.25	1.00	0.75	0.50	0.35
0.0	-0.469	-0.469	-0.469	-0.469	-0.469	-0.469
0.1	-0.475	-0.470	-0.464			
0.2	-0.476	-0.465	-0.451			
0.3	-0.472	-0.453	-0.416	-0.336	-0.144	0.174
0.4	-0.460	-0.425	-0.343	-0.183	0.120	0.545
0.5	-0.440	-0.379	-0.237	0.028	0.435	0.910
0.6	-0.408	-0.318	-0.110	0.288	0.842	1.307
0.7	-0.364	-0.228	0.016	0.571	1.424	1.903

Table 14.2 Biaxiality ratio β for the Double-edge-cracked plate in tension.

15 Double-edge-cracked circular disk

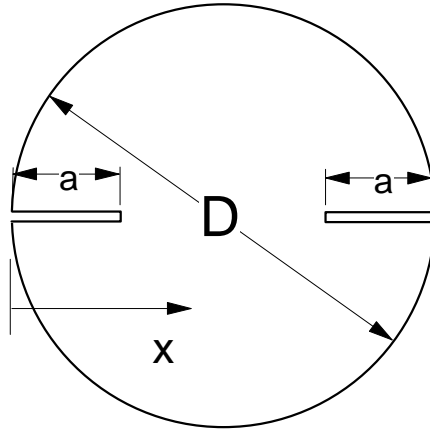


Fig. 15.1 Double-edge-cracked disk.

Figure 15.1 shows the double-edge-cracked disk. The T-stress under loading by constant circumferential normal tractions σ_n is shown in Fig. 15.2 together with the biaxiality ratio β . In contrast to the single-edge-cracked disk the relative crack length is defined here by $\alpha = a/R$ ($R = D/2$).

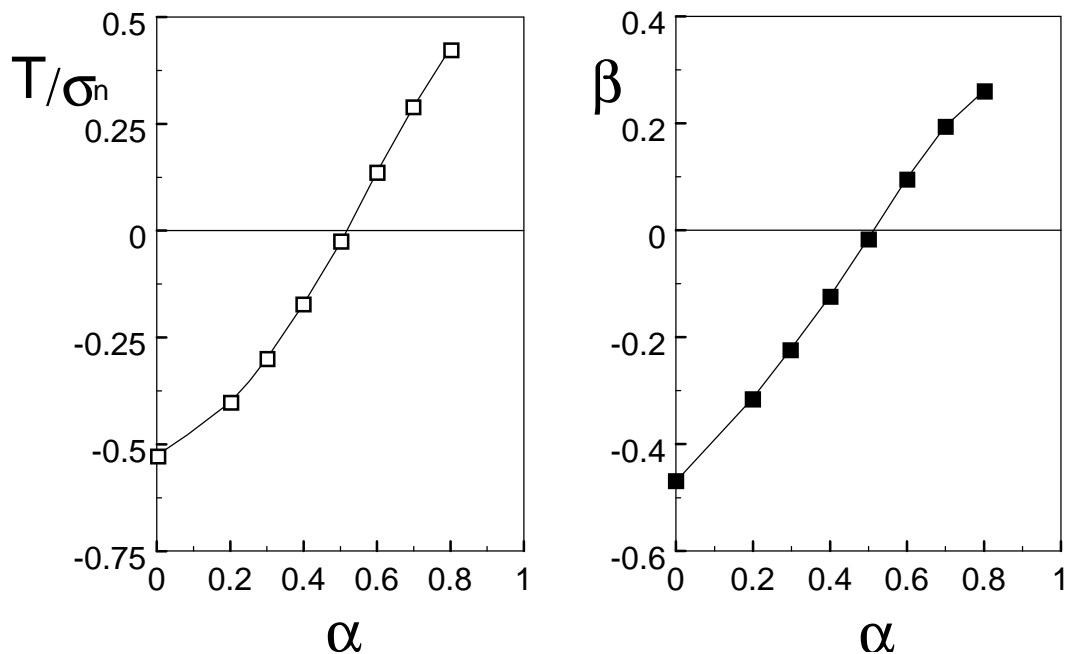


Fig. 15.2 T-stress and biaxiality ratio for the double-edge-cracked circular disk under circumferential normal tractions.

α	T/σ_n	β	$a \cdot C$
0	-0.526	-0.469	0.9481
0.2	-0.401	-0.316	1.199
0.3	-0.298	-0.224	1.405
0.4	-0.171	-0.125	1.658
0.5	-0.023	-0.016	1.954
0.6	0.136	0.095	2.273
0.7	0.290	0.194	2.580
0.8	0.425	0.260	2.850

Table 15.1 T-stress, biaxiality ratio and coefficient for the Green's function.
Loading: constant circumferential normal tractions

The T-stress entered into Table 15.1 can be expressed by

$$\frac{T}{\sigma_n} = -0.526 + 0.4022\alpha + 0.9104\alpha^2 + 1.4406\alpha^3 - 1.6874\alpha^4 \quad (15.1)$$

For the Green's function under symmetrical loading the same set-up is chosen as used for single-edge-cracked components, namely, expressed in the integrated form

$$T = C \int_0^a (1 - x/a) \sigma_y(x) dx - \sigma_y \Big|_{x=a} \quad (15.2)$$

with the parameter C entered into Table 15.1 and fitted for $\alpha \leq 0.8$ by the polynomial

$$C = \frac{1}{a} (0.9481 + 0.8043\alpha + 1.8207\alpha^2 + 2.8813\alpha^3 - 3.3747\alpha^4) \quad (15.3)$$

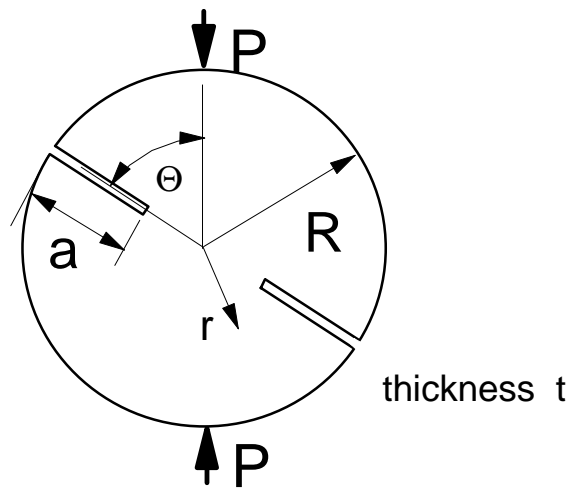


Fig. 15.3 Brazilian disk test with double-edge-cracked specimen.

Using the Green's function and the stress distribution given by eqs.(11.15) and (11.16) the T-stress was computed for the Brazilian disk test with double-edge-cracked disks. Table 15.2 contains the data for several angles Θ (see Fig. 15.3)

$\alpha = a/R$	$\Theta = \pi/32$	$\pi/16$	$\pi/8$	$\pi/4$	$3\pi/8$	$7\pi/16$	$\pi/2$
0	0	0	0	0	0	0	0
0.1	2.400	2.671	1.086	0.359	0.215	0.191	0.184
0.2	-1.946	0.900	1.453	0.711	0.458	0.413	0.399
0.3	-2.951	-0.917	0.0942	0.958	0.711	0.656	0.639
0.4	-3.185	-1.884	0.081	1.018	0.946	0.907	0.893
0.5	-3.226	-2.370	-0.716	0.867	1.129	1.142	1.143
0.6	-3.190	-2.610	-1.317	0.557	1.229	1.336	1.367
0.7	-3.100	-2.703	-1.72	0.177	1.232	1.459	1.531
0.8	-2.955	-2.688	-1.95	-0.179	1.148	1.493	1.608

Table 15.2 T-stress T/σ^* for the Brazilian disk test ($\sigma^*=2P/(\pi R)$).

16 References

- [1] Larssen, S.G., Carlsson, A.J., *J. of Mech. and Phys. of Solids* **21**(1973), 263-277
- [2] Sumpter, J.D., The effect of notch depth and orientation on the fracture toughness of multipass weldments, *Int. J. Press. Ves. and Piping* **10**(1982), 169-180
- [3] Cotterell, B., Li, Q.F., Zhang, D.Z., Mai, Y.W., On the effect of plastic constraint on ductile tearing in a structural steel, *Eng. Fract. Mech.* **21**(1985), 239-244.
- [4] Leever, P.S., Radon, J.C., Inherent stress biaxiality in various fracture specimen geometries, *Int. J. Fract.* **19**(1982), 311-325.
- [5] Kfoury, A.P., Some evaluations of the elastic T-term using Eshelby's method, *Int. J. Fract.* **30**(1986), 301-315.
- [6] Sham, T.L., The theory of higher order weight functions for linear elastic plane problems, *Int. J. Solids and Struct.* **25**(1989), 357-380.
- [7] Sham, T.L., The determination of the elastic T-term using higher order weight functions, *Int. J. Fract.* **48**(1991), 81-102.
- [8] Fett, T., A Green's function for T-stresses in an edge-cracked rectangular plate, *Eng. Fract. Mech.* **57**(1997), 365-373.
- [9] Fett, T., Munz, D., *Stress intensity factors and weight functions*, Computational Mechanics Publications, Southampton, 1997.
- [10] Wang, Y.Y., Parks, D.M., Evaluation of the elastic T-stress in surface-cracked plates using the line-spring method, *Int. J. Fract* **56**(1992), 25-40.
- [11] Fett, T., T-stress in edge-cracked specimens, FZKA 5802, Forschungszentrum Karlsruhe, 1996.
- [12] Fett, T., Stress intensity factors, T-stress and weight functions for double-edge-cracked plates, FZKA 5838, Forschungszentrum Karlsruhe, 1996.
- [13] Fett, T., T-stresses for internally cracked components, FZKA 6026, Forschungszentrum Karlsruhe, 1997.
- [14] Williams, M.L., On the stress distribution at the base of a stationary crack, *J. Appl. Mech.* **24**(1957), 109-114.
- [15] Bückner, H., A novel principle for the computation of stress intensity factors, *ZAMM* **50**(1970), 529-546.
- [16] Irwin, G.R., Analysis of stresses and strains near the end of a crack transversing a plate, *J. Appl. Mech.* **24**(1957), 361-364.
- [17] Gröbner, W., Hofreiter, N., *Integraltafel, Teil 1*, Springer Verlag, Wien New York, 1975.
- [18] Gross, B., Srawley, J.E., Brown, W.F., Stress intensity factors for a single-edge-notched tension specimen by Boundary Collocation of a stress function, NASA, Technical Note, D-2395, 1965.
- [19] Gross, B., Srawley, W.F., Stress intensity factors for a single-edge-notched tension specimen by Boundary Collocation of a stress function, NASA, Technical Note, D-2395, 1965.
- [20] Newman, J.C., An improved method of collocation for the stress analysis of cracked plates with various shaped boundaries, NASA TN D-6376, 1971.
- [21] Filon, L.N.G., On an approximate solution for the bending of a beam of rectangular cross-section under any system of load, with special reference to points of concentrated or discontinuous loading, *Phil. Trans., A*, **201**(1903), 63-155.

- [22] Rödel, J., Kelly, J.F., Lawn, B.R., In situ measurements of bridge crack interfaces in the scanning electron microscope, *J. Am. Ceram. Soc.* **73**(1990), 3313-3318.
- [23] Schneider, G.A., Magerl, F., Hahn, I., Petzow, G., In-situ observations of unstable and stable crack propagation and R-curve behaviour in thermally loaded disks, in: G.A. Schneider, G. Petzow (eds.), *Thermal Shock and Thermal Fatigue Behaviour of Advanced Ceramics*, 105-117, 1993 Kluwer Academic Publishers, Dordrecht, Netherlands.
- [24] Wigglesworth, L.A., Stress distribution in a notched plate, *Mathematica* **4**(1957), 76-96.
- [25] Atkinson, C., Smelser, R.E., Sanchez, J., Combined mode fracture via the cracked Brazilian disk test, *Int. J. Fract.* **18**(1982), 279-291
- [26] Creager, M., Paris, P.C., Elastic field equations for blunt cracks with reference to stress corrosion cracking, *Int. J. Fract.* **3**(1967), 247-252.
- [27] Tada, H., Paris, P.C., Irwin, G.R., *The stress analysis of cracks handbook*, Del Research Corporation, 1986.